Dinitrogen Cleavage by Three-Coordinate Molybdenum(III) Complexes: Mechanistic and Structural Data1

ARTICLE *in* JOURNAL OF THE AMERICAN CHEMICAL SOCIETY · SEPTEMBER 1996

Impact Factor: 12.11 · DOI: 10.1021/ja960574x

8 AUTHORS, INCLUDING:

Aaron L Odom
Michigan State University
83 PUBLICATIONS **3,039** CITATIONS
SEE PROFILE

Graham N George
University of Saskatchewan
292 PUBLICATIONS **10,199** CITATIONS
SEE PROFILE

Ingrid Pickering
University of Saskatchewan
197 PUBLICATIONS **8,332** CITATIONS
SEE PROFILE

Dinitrogen Cleavage by Three-Coordinate Molybdenum(III) Complexes: Mechanistic and Structural Data[1]

Catalina E. Laplaza,[†] Marc J. A. Johnson,[†] Jonas C. Peters,[†] Aaron L. Odom,[†] Esther Kim,[†] Christopher C. Cummins,*[,†] Graham N. George,*[,‡] and Ingrid J. Pickering[‡]

Contribution from the Department of Chemistry, Massachusetts Institute of Technology, 77 Massachusetts Avenue, Cambridge, Massachusetts 02139-4307, and Stanford Synchrotron Radiation Laboratory, SLAC, Stanford University, P.O. Box 4349, MS 69, Stanford, California 94309-0210

Received February 22, 1996[⊗]

Abstract: The synthesis and characterization of the complexes $Mo[N(R)Ar]_3$ ($R = C(CD_3)_2CH_3$, $Ar = 3,5\text{-}C_6H_3Me_2$), $(\mu\text{-}N_2)\{Mo[N(R)Ar]_3\}_2$, $(\mu\text{-}^{15}N_2)\{Mo[N(R)Ar]_3\}_2$, $NMo[N(R)Ar]_3$, $^{15}NMo[N(R)Ar]_3$, $Mo[N(t\text{-}Bu)Ph]_3$, $(\mu\text{-}N_2)\{Mo[N(t\text{-}Bu)Ph]_3\}_2$, and $NMo[N(t\text{-}Bu)Ph]_3$ are described. Temperature-dependent magnetic susceptibility data indicate a quartet ground state for $Mo[N(R)Ar]_3$. Single-crystal X-ray diffraction studies for $Mo[N(R)Ar]_3$ and $NMo[N(t\text{-}Bu)Ph]_3$ are described. Extended X-ray absorption fine structure (EXAFS) structural studies for $Mo[N(R)Ar]_3$, $(\mu\text{-}N_2)\{Mo[N(R)Ar]_3\}_2$, and $NMo[N(R)Ar]_3$ are reported. Temperature-dependent kinetic data are given for the unimolecular fragmentation of $(\mu\text{-}N_2)\{Mo[N(R)Ar]_3\}_2$ to 2 equiv of $NMo[N(R)Ar]_3$ and for the fragmentation of $(\mu\text{-}^{15}N_2)\{Mo[N(R)Ar]_3\}_2$ to 2 equiv of $^{15}NMo[N(R)Ar]_3$. The temperature dependence of the $^{15}N_2$ isotope effect for the latter N_2 cleavage process was fitted to a simple harmonic model, leading to a prediction for the difference in NN stretching frequencies for the two isotopomers. The latter prediction was consistent with the Raman spectroscopic data for $(\mu\text{-}N_2)\{Mo[N(R)Ar]_3\}_2$ and $(\mu\text{-}^{15}N_2)\{Mo[N(R)Ar]_3\}_2$. The Raman spectroscopic data and EXAFS results are both consistent with an NN bond order of approximately 2 in $(\mu\text{-}N_2)\{Mo[N(R)Ar]_3\}_2$. Temperature-dependent magnetic susceptibility data consistent with a triplet ground state are given for $(\mu\text{-}N_2)\{Mo[N(t\text{-}Bu)Ph]_3\}_2$.

Introduction

It was shown recently that the three-coordinate molybdenum(III) complex $Mo[N(R)Ar]_3$ [$R = C(CD_3)_2CH_3$, $Ar = 3,5\text{-}C_6H_3Me_2$][2] reacts readily with dinitrogen (1 atm, −35 to 30 °C) to provide the terminal nitrido complex $NMo[N(R)Ar]_3$,[3] via an intermediate formulated as $(\mu\text{-}N_2)\{Mo[N(R)Ar]_3\}_2$ (Scheme 1). Experiments utilizing $^{15}N_2$ established dinitrogen as the origin of the terminal nitrido nitrogen atom. The reaction (Scheme 1) is without precedent in its operational simplicity,[4] and the details of its mechanism are of inherent interest.[5] This molybdenum-based N_2 cleavage system is amenable to molecular-level scrutiny of both the N_2-binding and NN bond cleavage processes, rendering it unique among those nitrogenase models that synthetic chemists have yet developed.[6−8] Given the intense scrutiny to which dinuclear μ-dinitrogen complexes have been subjected,[9] it is gratifying that an N_2-cleavage reaction clearly stemming from such a species is now available for study.

This paper is concerned with those details of N_2 cleavage by $Mo[N(R)Ar]_3$ that are currently in hand, focusing primarily on details relevant to the NN bond cleavage step. Synthetic, structural, and magnetic data are given for three-coordinate $Mo[N(R)Ar]_3$, along with synthetic and characterization data for a new analog, $Mo[N(t\text{-}Bu)Ph]_3$. Structural characterization by extended X-ray absorption fine structure (EXAFS)[10] of the thermally-unstable purple intermediate, $(\mu\text{-}N_2)\{Mo[N(R)Ar]_3\}_2$ is reported. Also given are EXAFS data for three-coordinate $Mo[N(R)Ar]_3$ and the nitrido complex $NMo[N(R)Ar]_3$. The synthesis and single-crystal X-ray structure of the new terminal nitrido complex $NMo[N(t\text{-}Bu)Ph]_3$ are described. Temperature-dependent kinetic studies bearing on the conversion of purple $(\mu\text{-}N_2)\{Mo[N(R)Ar]_3\}_2$ to 2 equiv of $NMo[N(R)Ar]_3$ are reported and interpreted. Temperature-dependent kinetic studies of the conversion of $(\mu\text{-}^{15}N_2)\{Mo[N(R)Ar]_3\}_2$ to 2 equiv of $^{15}NMo[N(R)Ar]_3$, carried out to determine the heavy-atom isotope effect associated with the NN-cleavage step, are reported. Also described is a Raman spectroscopic study of purple $(\mu\text{-}N_2)\{Mo[N(R)Ar]_3\}_2$ and its isotopomer $(\mu\text{-}^{15}N_2)\{Mo[N(R)Ar]_3\}_2$, carried out to address the issue of the NN bond order in these species independent of the EXAFS information. The earlier assertion (based on ^2H NMR data) that purple $(\mu\text{-}N_2)\{Mo[N(R)Ar]_3\}_2$ is paramagnetic with a triplet ground state[3] is here substantiated via a temperature-dependent study of the magnetic susceptibility of $(\mu\text{-}N_2)\{Mo[N(t\text{-}Bu)Ph]_3\}_2$.

[†] Massachusetts Institute of Technology.

[‡] Stanford University.

[⊗] Abstract published in *Advance ACS Abstracts,* August 1, 1996.

(1) Dedicated to Professor Alan Davison of the MIT Department of Chemistry on the occasion of his 60th birthday.

(2) Laplaza, C. E.; Odom, A. L.; Davis, W. M.; Cummins, C. C.; Protasiewicz, J. D. *J. Am. Chem. Soc.* **1995**, *117*, 4999. Laplaza, C. E.; Davis, W. M.; Cummins, C. C. *Angew. Chem., Int. Ed. Engl.* **1995**, *34*, 2042.

(3) Laplaza, C. E.; Cummins, C. C. *Science* **1995**, *268*, 861. See also: Laplaza, C. E.; Johnson, A. R.; Cummins, C. C. *J. Am. Chem. Soc.* **1996**, *118*, 709.

(4) Leigh, G. J. *Science* **1995**, *268*, 827.

(5) The mechanism of dinitrogen cleavage by d^3 molybdenum and tungsten complexes was the subject of a recent theoretical study: Cui, Q.; Musaev, D. G.; Svensson, M.; Sieber, S.; Morokuma, K. *J. Am. Chem. Soc.* **1995**, *117*, 12366.

(6) Elegant structural models for the nitrogenase active site have been synthesized: Nordlander, E.; Lee, S. C.; Cen, W.; Wu, Z. Y.; Natoli, C. R.; Di Cicco, A.; Filipponi, A.; Hedman, B.; Hodgson, K. O.; Holm, R. H. *J. Am. Chem. Soc.* **1993**, *115*, 5549. For general reviews of transition metal dinitrogen complexes, see: Allen, A. D.; Harris, R. O.; Loescher, B. R.; Stevens, J. R.; Whiteley, R. N. *Chem. Rev.* **1973**, *73*, 11. Chatt, J.; Dilworth, J. R.; Richards, R. L. *Chem. Rev.* **1978**, *78*, 589. Henderson, R. A.; Leigh, G. J.; Pickett, C. J. *Adv. Inorg. Chem. Radiochem.* **1983**, *27*, 197. Leigh, G. J. *Acc. Chem. Res.* **1992**, *25*, 177. Leigh, G. J. *New J. Chem.* **1994**, *18*, 157. Hidai, M.; Mizobe, Y. *Chem. Rev.* **1995**, *95*, 1115.

S0002-7863(96)00574-4 CCC: $12.00

Results and Discussion

(i) Design, Synthesis, and Characterization of Mo[N(R)Ar]$_3$. The choice of the N[R]Ar ligand for the synthesis of an isolable, three-coordinate molybdenum(III) complex was premised on a number of considerations. *N-tert*-Butylarylamido ligands such as N[R]Ar are sterically[11] and electronically[12] comparable to the bis(trimethylsilyl)amido ligand. The bis(trimethylsilyl)amido ligand is noteworthy for the large number of three-coordinate M[N(SiMe$_3$)$_2$]$_3$ complexes it stabilizes both for the first-row transition metals[13] and for uranium.[14] Nonetheless, the bis(trimethylsilyl)amido ligand has well-documented shortcomings as an ancillary ligand, including its susceptibility to cyclometalation[15] and SiN bond cleavage[16] processes. The latter Achilles' heels are presumably responsible, at least in part, for the conspicuous absence of any second- or third-row transition metal M[N(SiMe$_3$)$_2$]$_3$ complexes. Radical ligand degradation processes should also be considered in this context.[17] It was our hope that N[R]Ar and related ligands would emulate the beneficial aspects accordant to N(SiMe$_3$)$_2$ without manifesting its shortcomings. A potential further benefit of *N-tert*-butylarylamido ligands is the wide range of substituted anilines available for their preparation,[18] which should permit electronic tuning of reactivity.[19] Finally, the ready incorporation of a deuterium NMR handle into the N[R]Ar ligand has facilitated the preparation of paramagnetic complexes including Mo[N(R)Ar]$_3$, by virtue of the fact that, for paramagnetic complexes, ^{2}H NMR lines are substantially narrower than corresponding ^{1}H NMR signals.[20] Complexes containing the N[R]Ar ligand exhibit one ^{2}H NMR signal for each unique ligand environment, making ^{2}H NMR a rapid and convenient method for assaying paramagnetic reaction mixtures.

As communicated previously,[2] Mo[N(R)Ar]$_3$ is obtained as an orange-red crystalline solid in 70% yield upon treatment of *mer*-MoCl$_3$(THF)$_3$[21] with 2 equiv of Li[N(R)Ar](OEt$_2$)[22] in ether (see the Experimental Section for preparative details). To avoid contamination with the dinuclear dinitrogen complex (μ-N$_2$)-{Mo[N(R)Ar]$_3$}$_2$ or with NMo[N(R)Ar]$_3$, Mo[N(R)Ar]$_3$ is purified by recrystallization under an argon atmosphere at −35 °C. A typical preparation yields ca. 1.5 g of Mo[N(R)Ar]$_3$. The compound exhibits a diagnostic ^{2}H NMR resonance at ca. 64 ppm for its deuterated *tert*-butyl groups. The proton NMR spectrum of Mo[N(R)Ar]$_3$ exhibits the expected four broad

(7) Recent reports involving mononuclear molybdenum and tungsten dinitrogen complexes: Oshita, H.; Mizobe, Y.; Hidai, M. *J. Organomet. Chem.* **1993**, *456*, 213. Seino, H.; Ishii, Y.; Hidai, M. *J. Am. Chem. Soc.* **1994**, *116*, 7433. Ishii, Y.; Kawaguchi, M.; Ishino, Y.; Aoki, T.; Hidai, M. *Organometallics* **1994**, *13*, 5062. Baker, R. T.; Calabrese, J. C.; Harlow, R. L.; Williams, I. D. *Organometallics* **1993**, *12*, 830. Fernández-Trujillo, M. J.; Basallote, M. G.; Valerga, P.; Puerta, M. C. *J. Chem. Soc., Dalton Trans.* **1993**, 923. Jiménez-Tenorio, M.; Puerta, M. C.; Valerga, P.; Hughes, D. L. *J. Chem. Soc., Dalton Trans.* **1994**, 2431. Hughes, D. L.; Ibrahim, S. K.; Pickett, C. J.; Querne, G.; Laouenan, A.; Talarmin, J.; Queiros, A.; Fonseca, A. *Polyhedron* **1994**, *13*, 3341. George, T. A.; Kaul, B. B.; Chen, Q.; Zubieta, J. *Inorg. Chem.* **1993**, *32*, 1706. Dzięgielewski, J. O.; Małecki, J. G.; Grzybek, R. *Polyhedron* **1994**, *13*, 241. Luo, X.-L.; Kubas, G. J.; Burns, C. J.; Eckert, J. *Inorg. Chem.* **1994**, *33*, 5219. Recent reports involving mononuclear rhenium dinitrogen complexes: Orth, S. D.; Barrera, J.; Sabat, M.; Harman, W. D. *Inorg. Chem.* **1994**, *33*, 3026. Dilworth, J. R.; Hu, J.; Miller, J. R.; Hughes, D. L.; Zubieta, J. A.; Chen, Q. *J. Chem. Soc., Dalton Trans.* **1995**, 3153. Cusanelli, A.; Sutton, D. *Organometallics* **1995**, *14*, 4651. Richards, T. C.; Bard, A. J.; Cusanelli, A.; Sutton, D. *Organometallics* **1994**, *13*, 757. Wang, Y.; Da Silva, J. J. R. F.; Pombeiro, A. J. L.; Pellinghelli, M. A.; Tiripicchio, A. *J. Organomet. Chem.* **1993**, *454*, 211. Recent reports involving mononuclear iron dinitrogen complexes: Hills, A.; Hughes, D. L.; Jiménez-Tenorio, M.; Leigh, G. J.; Rowley, A. T. *J. Chem. Soc., Dalton Trans.* **1993**, 3041. Hughes, D. L.; Leigh, G. J.; Jiménez-Tenorio, M.; Rowley, A. T. *J. Chem. Soc., Dalton Trans.* **1993**, 75. Perthuisot, C.; Jones, W. D. *New J. Chem.* **1994**, *18*, 621. Komiya, S.; Akita, M.; Yoza, A.; Kasuga, N.; Fukuoka, A.; Kai, Y. *J. Chem. Soc., Chem. Commun.* **1993**, 787. de la Jara Leal, A.; Jiménez-Tenorio, M.; Puerta, M. C.; Valerga, P. *Organometallics* **1995**, *14*, 3839. Recent reports involving mononuclear ruthenium and osmium dinitrogen complexes: Li, Z.-W.; Harman, W. D.; Lay, P. A.; Taube, H. *Inorg. Chem.* **1994**, *33*, 3635. Filipek, K. *Inorg. Chim. Acta* **1995**, *231*, 237. Bianchini, C.; Linn, K.; Masi, D.; Peruzzini, M.; Polo, A.; Vacca, A.; Zanobini, F. *Inorg. Chem.* **1993**, *32*, 2366. Rao, N. N. *J. Mol. Catal.* **1994**, *93*, 23. Takahashi, T.; Hiratani, K.; Kimura, E. *Chem. Lett.* **1993**, 1329.

(8) Catalytic nitrogen-fixing systems: Antipin, M.; Struchkov, Y.; Shilov, A.; Shilova, A. *Gazz. Chim. Ital.* **1993**, *123*, 265. Luneva, N. P.; Mironova, S. A.; Shilov, A. E.; Antipin, M. Y.; Struchkov, Y. T. *Angew. Chem., Int. Ed. Engl.* **1993**, *32*, 1178. Shilov, A. E. *Pure Appl. Chem.* **1992**, *64*, 1409.

(9) Dititanium μ-dinitrogen complexes: (a) Berry, D. H.; Procopio, L. J.; Carroll, P. J. *Organometallics* **1988**, *7*, 570. (b) Duchateau, R.; Gambarotta, S.; Beydoun, N.; Bensimon, C. *J. Am. Chem. Soc.* **1991**, *113*, 8986. (c) Beydoun, N.; Duchateau, R.; Gambarotta, S. *J. Chem. Soc., Chem. Commun.* **1992**, 244. (d) Sanner, R. D.; Duggan, D. M.; McKenzie, T. C.; Marsh, R. E.; Bercaw, J. E. *J. Am. Chem. Soc.* **1976**, *98*, 8358. (e) Zeinstra, J. D.; Teuben, J. H.; Jellinek, F. *J. Organomet. Chem.* **1979**, *170*, 39. Dizirconium μ-dinitrogen complexes: (f) Sanner, R. D.; Manriquez, J. M.; Marsh, R. E.; Bercaw, J. E. *J. Am. Chem. Soc.* **1976**, *98*, 8351. (g) Fryzuk, M. D.; Haddad, T. S.; Mylvaganam, M.; McConville, D. H.; Rettig, S. J. *J. Am. Chem. Soc.* **1993**, *115*, 2782. (h) Cohen, J. D.; Mylvaganam, M.; Fryzuk, M. D.; Loehr, T. M. *J. Am. Chem. Soc.* **1994**, *116*, 9529. Divanadium μ-dinitrogen complexes: (i) Edema, J. J. H.; Meetsma, A.; Gambarotta, S. *J. Am. Chem. Soc.* **1989**, *111*, 6878. (j) Song, J.-I.; Berno, P.; Gambarotta, S. *J. Am. Chem. Soc.* **1994**, *116*, 6927. (k) Berno, P.; Hao, S.; Minhas, R.; Gambarotta, S. *J. Am. Chem. Soc.* **1994**, *116*, 7417. (l) Buijink, J.-K. F.; Meetsma, A.; Teuben, J. H. *Organometallics* **1993**, *12*, 2004. (m) Ferguson, R.; Solari, E.; Floriani, C.; Chiesi-Villa, A.; Rizzoli, C. *Angew. Chem., Int. Ed. Engl.* **1993**, *32*, 396. Diniobium μ-dinitrogen complexes: (n) Dilworth, J. R.; Henderson, R. A.; Hills, A.; Hughes, D. L.; Macdonald, C.; Stephens, A. N.; Walton, D. R. M. *J. Chem. Soc., Dalton Trans.* **1990**, 1077. (o) Berno, P.; Gambarotta, S. *Organometallics* **1995**, *14*, 2159. Ditantalum μ-dinitrogen complexes: (p) Turner, H. W.; Fellmann, J. D.; Rocklage, S. M.; Schrock, R. R.; Churchill, M. R.; Wasserman, H. J. *J. Am. Chem. Soc.* **1980**, *102*, 7809. (q) Rocklage, S. M.; Turner, H. W.; Fellmann, J. D.; Schrock, R. R. *Organometallics* **1982**, *1*, 703. (r) Rocklage, S. M.; Schrock, R. R. *J. Am. Chem. Soc.* **1982**, *104*, 3077. (s) Churchill, M. R.; Wasserman, H. J. *Inorg. Chem.* **1981**, *20*, 2899. (t) Churchill, M. R.; Wasserman, H. J. *Inorg. Chem.* **1982**, *21*, 218. (u) Schrock, R. R.; Wesolek, M.; Liu, A. H.; Wallace, K. C.; Dewan, J. C. *Inorg. Chem.* **1988**, *27*, 2050. Dichromium μ-dinitrogen complexes: (v) Denholm, S.; Hunter, G.; Weakley, T. J. R. *J. Chem. Soc., Dalton Trans.* **1987**, 2789. Dimolybdenum μ-dinitrogen complexes: (w) Forder, R. A.; Prout, K. *Acta Crystallogr.* **1974**, *B30*, 2778. (x) Schrock, R. R.; Kolodziej, R. M.; Liu, A. H.; Davis, W. M.; Vale, M. G. *J. Am. Chem. Soc.* **1990**, *112*, 4338. (y) Kol, M.; Schrock, R. R.; Kempe, R.; Davis, W. M. *J. Am. Chem. Soc.* **1994**, *116*, 4382. (z) Shih, K.-Y.; Schrock, R. R.; Kempe, R. *J. Am. Chem. Soc.* **1994**, *116*, 8804. (aa) Luo, X.-L.; Kubas, G. J.; Burns, C. J.; Butcher, R. J.; Bryan, J. C. *Inorg. Chem.* **1995**, *34*, 6538. Ditungsten μ-dinitrogen complexes: (bb) Anderson, S. N.; Richards, R. L.; Hughes, D. L. *J. Chem. Soc., Chem. Commun.* **1982**, 1291. (cc) Anderson, S. N.; Richards, R. L.; Hughes, D. L. *J. Chem. Soc., Dalton Trans.* **1986**, 245. (dd) Churchill, M. R.; Li, Y.-J.; Theopold, K. H.; Schrock, R. R. *Inorg. Chem.* **1984**, *23*, 4472. (ee) Murray, R. C.; Schrock, R. R. *J. Am. Chem. Soc.* **1985**, *107*, 4557. (ff) Churchill, M. R.; Li, Y.-J. *J. Organomet. Chem.* **1986**, *301*, 49. (gg) O'Regan, M. B.; Liu, A. H.; Finch, W. C.; Schrock, R. R.; Davis, W. M. *J. Am. Chem. Soc.* **1990**, *112*, 4331. (hh) Harlan, C. J.; Jones, R. A.; Koschmieder, S. U.; Nunn, C. M. *Polyhedron* **1990**, *9*, 669. Dimanganese and ditechnetium μ-dinitrogen complexes: (ii) Weidenhammer, K.; Herrmann, W. A.; Ziegler, M. L. *Z. Anorg. Allg. Chem.* **1979**, *457*, 183. (jj) Joachim, J. E.; Apostolidis, C.; Kanellakopulos, B.; Maier, R.; Meyer, D.; Rebizant, J.; Ziegler, M. L. *J. Organomet. Chem.* **1993**, *455*, 137. Dinuclear μ-dinitrogen complexes of iron, ruthenium, or osmium: (kk) Berke, H.; Bankhardt, W.; Huttner, G.; von Seyerl, J.; Zsolnai, L. *Chem. Ber.* **1981**, *114*, 2754. (ll) Che, C.-M.; Lam, H.-W.; Tong, W.-F.; Lai, T.-F.; Lau, T.-C. *J. Chem. Soc., Chem. Commun.* **1989**, 1883. (mm) Sellmann, D.; Friedrich, H.; Knoch, F.; Moll, M. *Z. Naturforsch.* **1994**, *49b*, 76. Dinuclear μ-dinitrogen complexes of cobalt, rhodium, or iridium: (nn) Cecconi, F.; Ghilardi, C. A.; Midollini, S.; Moneti, S.; Orlandini, A.; Bacci, M. *J. Chem. Soc., Chem. Commun.* **1985**, 731. (oo) Klein, H.-F.; Beck, H.; Hammerschmitt, B.; Koch, U.; Koppert, S.; Cordier, G. *Z. Naturforsch.* **1991**, *B46*, 147. (pp) Yoshida, T.; Okano, T.; Thorn, D. L.; Tulip, T. H.; Otsuka, S.; Ibers, J. A. *J. Organomet. Chem.* **1979**, *181*, 183. (qq) Gutiérrez, E.; Monge, A.; Nicasio, M. C.; Poveda, M. L.; Carmona, E. *J. Am. Chem. Soc.* **1994**, *116*, 791. Dinickel μ-dinitrogen complexes: (rr) Jolly, P. W.; Jonas, K.; Krüger, C.; Tsay, Y.-H. *J. Organomet. Chem.* **1971**, *33*, 109. Mixed-metal μ-dinitrogen complexes: (ss) Mizobe, Y.; Yokobayashi, Y.; Oshita, H.; Takahashi, T.; Hidai, M. *Organometallics* **1994**, *13*, 3764. (tt) Mercer, M.; Crabtree, R. H.; Richards, R. L. *J. Chem. Soc., Chem. Commun.* **1973**, 808. (uu) Mercer, M. *J. Chem. Soc., Dalton Trans.* **1974**, 1637; see also ref 9x above.

Scheme 1

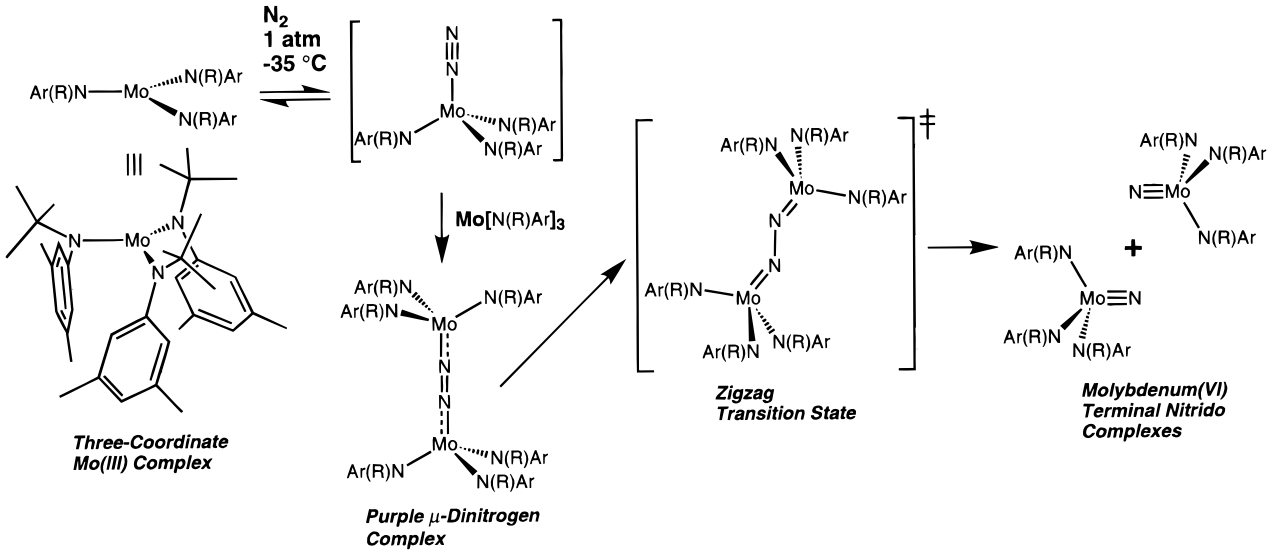

resonances, the sharpest of which is found at −9.6 ppm (C_6D_6, ca. 25 °C), which we assign to the meta methyl groups on the Ar residues. Solution magnetic susceptibility measurements obtained by the method of Evans[23] are consistent with a quartet ground state for $Mo[N(R)Ar]_3$ [$\mu_{eff} = 3.56\ \mu_B$].[2] SQUID magnetic susceptibility measurements for solid $Mo[N(R)Ar]_3$ yield a magnetic moment very close to the spin-only value for three unpaired electrons ($\mu_s = 3.87\ \mu_B$): the best least-squares fit of the data to the Curie−Weiss law gave $\mu = 3.82\ \mu_B$ over the temperature range 5−300 K (Figure 1; see Experimental Section for details).

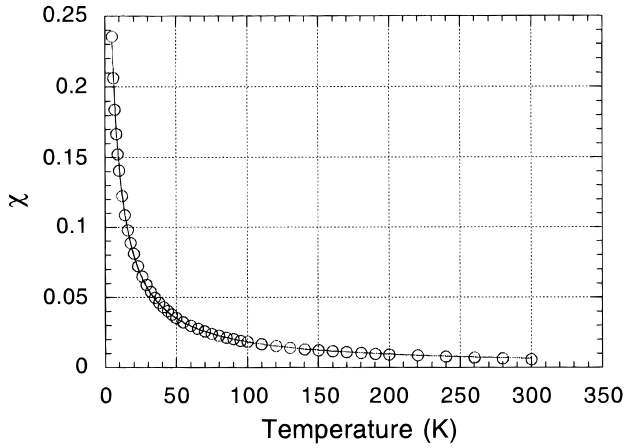

Figure 1. SQUID magnetic susceptibility data for solid $Mo(N[R]Ar)_3$ from 5 to 300 K fit to the Curie−Weiss law ($\mu = 3.82\ \mu_B$; see Experimental Section for details).

The new three-coordinate molybdenum(III) complex Mo[N(*t*-Bu)Ph]$_3$, obtained in ca. 55% yield as burgundy crystals, was prepared in a fashion analogous to $Mo[N(R)Ar]_3$ (see Experimental Section for details). ^{1}H NMR, magnetic susceptibility, and chemical reactivity data (*vide infra*) are consistent with formulation of Mo[N(*t*-Bu)Ph]$_3$ as a three-coordinate molybdenum(III) monomer.

(ii) Solid-State and Solution Structure of Mo[N(R)Ar]$_3$. The X-ray crystal structure of $Mo[N(R)Ar]_3$ was communicated previously in conjunction with a study on its cleavage of the nitrous oxide NN bond.[2] Salient features of the structure that should be borne in mind when considering reactions of this

(10) Cramer, S. P.; Hodgson, K. O. *Prog. Inorg. Chem.* **1979**, *25*, 1.

(11) Bradley has articulated the concept of steric saturation of the primary coordination sphere: Bradley, D. C. *Chem. Br.* **1975**, *11*, 393. Eller, P. G.; Bradley, D. C.; Hursthouse, M. B.; Meek, D. W. *Coord. Chem. Rev.* **1977**, *24*, 1.

(12) The NH pK_a for $HN(SiMe_3)_2$ has been given as 25.8 in tetrahydrofuran as ascertained using ^{13}C NMR methods; see: Fraser, R. R.; Mansour, T. S. *J. Org. Chem.* **1984**, *49*, 5284. Fraser, R. R.; Mansour, T. S. *J. Org. Chem.* **1984**, *49*, 3442.

(13) (a) Lappert, M. F.; Power, P. P.; Sanger, A. R.; Srivastava, R. C. *Metal and Metalloid Amides*; Ellis Horwood: Chichester, 1980. (b) Bradley, D. C.; Copperthwaite, R. G. *Inorg. Synth.* **1978**, *18*, 112. (c) Bradley, D. C.; Hursthouse, M. B.; Newing, C. W.; Welch, A. J. *J. Chem. Soc., Chem. Commun.* **1972**, 567. (d) Alyea, E. C.; Bradley, D. C.; Copperthwaite, R. G. *J. Chem. Soc., Dalton Trans.* **1972**, 1580. (e) Bradley, D. C.; Newing, C. W. *J. Chem. Soc., Chem. Commun.* **1970**, 219. (f) Bradley, D. C.; Hursthouse, M. B.; Rodesiler, P. F. *J. Chem. Soc., Chem. Commun.* **1969**, 14. (g) Ellison, J. J.; Power, P. P.; Shoner, S. C. *J. Am. Chem. Soc.* **1989**, *111*, 8044. (h) Bürger, H.; Wannagat, U. *Monatsh. Chem.* **1964**, *95*, 1099. (i) Bürger, H.; Wannagat, U. *Monatsh. Chem.* **1963**, *94*, 1007.

(14) (a) Andersen, R. A. *Inorg. Chem.* **1979**, *18*, 1507. (b) Van Der Sluys, W. G.; Burns, C. J.; Huffman, J. C.; Sattelberger, A. P. *J. Am. Chem. Soc.* **1988**, *110*, 5924. (c) Avens, L. R.; Bott, S. G.; Clark, D. L.; Sattelberger, A. P.; Watkin, J. G.; Zwick, B. D. *Inorg. Chem.* **1994**, *33*, 2248.

(15) Simpson, S. J.; Andersen, R. A. *Inorg. Chem.* **1981**, *20*, 3627. Simpson, S. J.; Andersen, R. A. *Inorg. Chem.* **1981**, *20*, 2991. Berno, P.; Gambarotta, S. *Angew. Chem., Int. Ed. Engl.* **1995**, *34*, 822. Berno, P.; Minhas, R.; Hao, S.; Gambarotta, S. *Organometallics* **1994**, *13*, 1052.

(16) Bürger, H.; Wannagat, U. *Monatsh. Chem.* **1963**, *94*, 761.

(17) We have encountered the following radical bond cleavage processes: $Mo^{V}OR \rightarrow M^{VI}O + [^{\bullet}R]$ and $Mo^{V}NRAr \rightarrow M^{VI}NAr + [^{\bullet}R]$, to be reported in due course. Peters, J.; Wanandi, P. W.; Odom, A. L.; Davis, W. M.; Cummins, C. C. *J. Am. Chem. Soc.*, in press. Johnson, A. R.; Odom, A. L.; Cummins, C. C. Manuscript in preparation.

(18) The 1992−1993 edition of the Aldrich Structure Index lists ca. 100 variously substituted anilines that conceivably could be employed in the synthesis of *N-tert*-butyl arylamido ligands.

(19) Schrock and co-workers have demonstrated exquisite control over the reactivity of molybdenum metathesis catalysts, of general formula Mo(NAr)(CHR)(OR′)$_2$, by varying the alkoxide substituent. See: Schrock, R. R. *Pure Appl. Chem.* **1994**, *66*, 1447 and references therein.

(20) La Mar, G. N.; Horrocks, W. DeW., Jr.; Holm, R. H. *NMR of Paramagnetic Molecules*; Academic Press: New York, 1973. Johnson, A.; Everett, G. W., Jr. *J. Am. Chem. Soc.* **1972**, *94*, 1419. Wheeler, W. D.; Kaizaki, S.; Legg, J. I. *Inorg. Chem.* **1982**, *21*, 3248. Hill, D. H.; Parvez, M. A.; Sen, A. *J. Am. Chem. Soc.* **1994**, *116*, 2889. Hill, D. H.; Sen, A. *J. Am. Chem. Soc.* **1988**, *110*, 1650. Li, Z.; Goff, H. M. *Inorg. Chem.* **1992**, *31*, 1547.

(21) We prepare orange *mer*-$MoCl_3(THF)_3$ according to Dilworth and Zubieta: Dilworth, J. R.; Zubieta, J. *Inorg. Synth.* **1986**, *24*, 193. For a paramagnetic ^{1}H NMR study of the solution stability of monomeric *mer*-$MoCl_3(THF)_3$, see: Poli, R.; Mui, H. D. *J. Am. Chem. Soc.* **1990**, *112*, 2446. For the single-crystal X-ray structure of *mer*-$MoCl_3(THF)_3$, see: Hofacker, P.; Friebel, C.; Dehnicke, K.; Bäuml, P.; Hiller, W.; Strähle, J. *Z. Naturforsch.* **1989**, *44b*, 1161.

(22) Laplaza, C. E.; Davis, W. M.; Cummins, C. C. *Organometallics* **1995**, *14*, 577.

(23) Sur, S. K. *J. Magn. Reson.* **1989**, *82*, 169. Evans, D. F. *J. Chem. Soc.* **1959**, 2003.

Table 1. Selected Bond Distances (Å) and Angles (deg) for $Mo(N[R]Ar)_3$

Mo−N(1)	1.960(7)	Mo(A)−N(1A)	1.970(7)
Mo−N(2)	1.964(7)	Mo(A)−N(2A)	1.968(7)
Mo−N(3)	1.977(7)	Mo(A)−N(3A)	1.956(7)
N(1)−C(11)	1.42(1)	N(1A)−C(11A)	1.42(1)
N(1)−C(17)	1.50(1)	N(1A)−C(17A)	1.48(1)
N(2)−C(21)	1.44(1)	N(2A)−C(21A)	1.43(1)
N(2)−C(27)	1.49(1)	N(2A)−C(27A)	1.49(1)
N(3)−C(31)	1.43(1)	N(3A)−C(31A)	1.43(1)
N(3)−C(37)	1.49(1)	N(3A)−C(37A)	1.48(1)
N(1)−Mo−N(2)	120.4(3)	N(1A)−Mo(A)−N(2A)	120.3(3)
N(1)−Mo−N(3)	118.0(3)	N(1A)−Mo(A)−N(3A)	120.0(3)
N(2)−Mo−N(3)	119.3(3)	N(2A)−Mo(A)−N(3A)	118.9(3)
Mo−N(1)−C(11)	110.2(5)	Mo(A)−N(1A)−C(11A)	108.6(6)
Mo−N(1)−C(17)	131.7(6)	Mo(A)−N(1A)−C(17A)	132.1(6)
C(11)−N(1)−C(17)	118.1(7)	C(11A)−N(1A)−C(17A)	118.8(8)
Mo−N(2)−C(21)	111.5(5)	Mo(A)−N(2A)−C(21A)	110.2(6)
Mo−N(2)−C(27)	130.7(6)	Mo(A)−N(2A)−C(27A)	130.7(6)
C(21)−N(2)−C(27)	117.7(7)	C(21A)−N(2A)−C(27A)	119.1(7)
Mo−N(3)−C(31)	108.9(5)	Mo(A)−N(3A)−C(31A)	110.4(6)
Mo−N(3)−C(37)	132.0(6)	Mo(A)−N(3A)−C(37A)	131.8(6)
C(31)−N(3)−C(37)	119.0(7)	C(31A)−N(3A)−C(37A)	117.8(7)

compound with small molecules include (i) a trigonal planar MoN_3 unit, (ii) amido NC_2 planes roughly perpendicular to the MoN_3 plane, (iii) *tert*-butyl groups occupying one hemisphere and aryl groups the other, and (iv) aryl residues oriented roughly perpendicular to their contiguous $MoNC_2$ planes (See Table 1 for selected bond lengths and angles). An ORTEP diagram and space-filling models, depicted in Figure 2, suggest that the most accessible approach to the Mo atom is a shallow channel bounded by the three *tert*-butyl groups (Figure 2c). A second channel, bounded by the three aryl groups (Figure 2d), presents a much deeper path to the Mo atom and should thus appear less enticing to an incoming small molecule. Three axial clefts (Figure 2b), which appear impossibly narrow, offer the only other access to the Mo atom. An expansion of the *tert*-butyl-bounded cavity upon penetration by a small molecule (e.g., N_2 or N_2O) appears to be required, on the basis of van der Waals radii considerations. Such an expansion should be accompanied by contraction of the aryl-bounded cavity on the opposing hemisphere, as discussed below in connection with the X-ray structure of NMo[N(*t*-Bu)Ph]$_3$. NMR (*vide supra*) and EXAFS (*vide infra*) data for $Mo[N(R)Ar]_3$ are consistent with an average 3-fold symmetric structure for the molecule in solution, as observed in the solid state. We have no evidence for a "two-up, one-down" structure as has been observed for trigonal bipyramidal tris(arylthiolate)ML_2 complexes (M = Tc, Re; L = e.g., acetonitrile).[24] Edge-to-face aryl interactions could contribute to the apparent preference for the observed "three-up" structure: metrical parameters for the lowest energy gas-phase structure of the benzene trimer[25] are strikingly similar to those for three aromatic rings oriented as in $Mo[N(R)Ar]_3$. A preliminary X-ray structure carried out for Mo[N(*t*-Bu)Ph]$_3$ has revealed that it is quite similar in shape to $Mo[N(R)Ar]_3$;[26] thus, no special structural significance should be attributed to the aryl methyl substituents in the latter complex.

(iii) Dinitrogen Binding by Mo[N(R)Ar]$_3$. The uptake of dinitrogen (at ca. 1 atm) by $Mo[N(R)Ar]_3$ (benzene, 28 °C, 3.5 mM) is a slow process, with ≤5% conversion to $NMo[N(R)Ar]_3$ observed in 12 h. The intermediate purple complex $(\mu\text{-}N_2)\{Mo[N(R)Ar]_3\}_2$ is not observed when the reaction is carried out at ca. 28 °C, presumably because at that temperature it converts rapidly to $NMo[N(R)Ar]_3$. A typical procedure for generating samples rich in purple $(\mu\text{-}N_2)\{Mo[N(R)Ar]_3\}_2$ involves storage of a ca. 0.05 M toluene solution of $Mo[N(R)Ar]_3$ in a glovebox refrigerator at ca. −35 °C for several (3−8) days. During this incubation period, the solution turns royal purple and, according to ^{2}H NMR monitoring, a single new species proposed to be $(\mu\text{-}N_2)\{Mo[N(R)Ar]_3\}_2$ (δ = 14 ppm) appears. Upon warming to 28 °C the purple color soon gives way to the amber color of $NMo[N(R)Ar]_3$, which according to ^{1}H and ^{2}H NMR analysis forms quantitatively, and which has been isolated from such reaction mixtures in 76% recrystallized yield. Solutions of $Mo[N(R)Ar]_3$ do not acquire a purple color, and do not exhibit the characteristic ^{2}H NMR resonance at 14 ppm, when cooled under argon instead of dinitrogen. The use of 1 atm of 99%-$^{15}N_2$ led to smooth production of the labeled complex $^{15}NMo[N(R)Ar]_3$, which has been characterized by infrared spectroscopy [ν(MoN) = 1014 cm^{-1} versus 1042 cm^{-1} for its unlabeled counterpart] and ^{15}N NMR spectroscopy (δ = +840 ppm[27]). Essentially identical spectroscopic properties were observed for $^{15}NMo[N(R)Ar]_3$ prepared independently from $Mo[N(R)Ar]_3$ and selectively-labeled $^{15}NNN(p\text{-}C_6H_4Me)$.[2] The putative mononuclear dinitrogen complex $(\eta^1\text{-}N_2)Mo[N(R)Ar]_3$ (Scheme 1), the logical immediate precursor to $(\mu\text{-}N_2)\{Mo[N(R)Ar]_3\}_2$ has not been observed. Apparently the equilibrium constant for dinitrogen capture by $Mo[N(R)Ar]_3$ is small under the conditions utilized.

(iv) X-ray Absorption Near-Edge Spectra and EXAFS of Mo[N(R)Ar]$_3$, (μ-N$_2$){Mo[N(R)Ar]$_3$}$_2$, and NMo[N(R)Ar]$_3$. The X-ray absorption near-edge spectra of $Mo[N(R)Ar]_3$, $(\mu\text{-}N_2)\{Mo[N(R)Ar]_3\}_2$, and $NMo[N(R)Ar]_3$ are shown in Figure 3. All of the spectra exhibit a relatively broad edge, as expected

(24) de Vries, N.; Dewan, J. C.; Jones, A. G.; Davison, A. *Inorg. Chem.* **1988**, *27*, 1574. de Vries, N.; Jones, A. G.; Davison, A. *Inorg. Chem.* **1989**, *28*, 3728. Blower, P. J.; Dilworth, J. R.; Hutchinson, J. P.; Zubieta, J. A. *J. Chem. Soc., Dalton Trans.* **1985**, 1533. Bishop, P. T.; Dilworth, J. R.; Hutchinson, J.; Zubieta, J. *J. Chem. Soc., Dalton Trans.* **1986**, 967. Dilworth, J. R.; Hutchinson, J.; Zubieta, J. A. *J. Chem. Soc., Chem. Commun.* **1983**, 1034. Koch, S. A.; Millar, M. *J. Am. Chem. Soc.* **1983**, *105*, 3362. For a "three-up" tris(arylthiolate) complex with acetonitrile lodged in the pocket bounded by aromatic residues, see: Dilworth, J. R.; Neaves, B. D.; Hutchinson, J. P.; Zubieta, J. A. *Inorg. Chim. Acta* **1982**, *65*, L223.

(25) The following papers deal with aspects of the structure and energetics of the benzene trimer: Kratzschmar, O.; Selzle, H. L.; Schlag, E. W. *J. Phys. Chem.* **1994**, *98*, 3501. Xiao, Y. L.; Williams, D. E. *Chem. Phys. Lett.* **1993**, *215*, 17. Henson, B. F.; Venturo, V. A.; Hartland, G. V.; Felker, P. M. *J. Chem. Phys.* **1993**, *98*, 8361. Krause, H.; Ernstberger, B.; Neusser, H. J. *Ber. Bunsen-Ges. Phys. Chem.* **1992**, *96*, 1183.

(26) Johnson, M. J. A.; Odom, A. L.; Cummins, C. C. Manuscript in preparation.

(27) The ^{15}N NMR shift is quoted with reference to external neat nitromethane, whose chemical shift is +380.2 ppm with respect to liquid NH_3 (taken as 0 ppm): von Philipsborn, W.; Müller, R. *Angew. Chem., Int. Ed. Engl.* **1986**, *25*, 383.

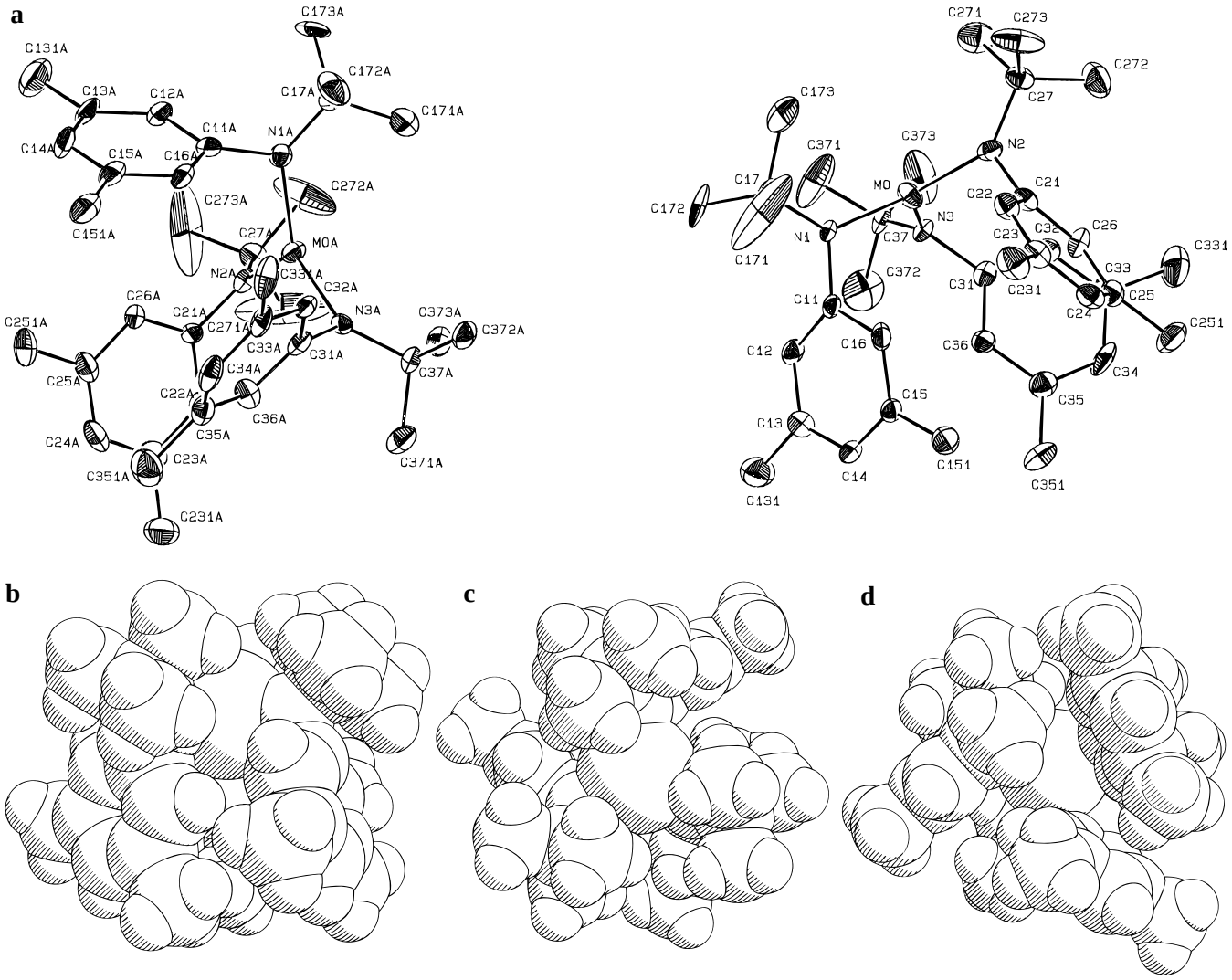

Figure 2. (a) Structural diagram and atom-labeling scheme for $Mo(N[R]Ar)_3$. Thermal ellipsoids are at the 35% probability level. Space-filling representations of $Mo(N[R]Ar)_3$ viewed (b) perpendicular to the N_3 plane normal, (c) along the N_3 plane normal facing the hemisphere protected by *tert*-butyl-d_6 groups, and (d) along the N_3 plane normal facing the hemisphere protected by 3,5-dimethylphenyl groups.

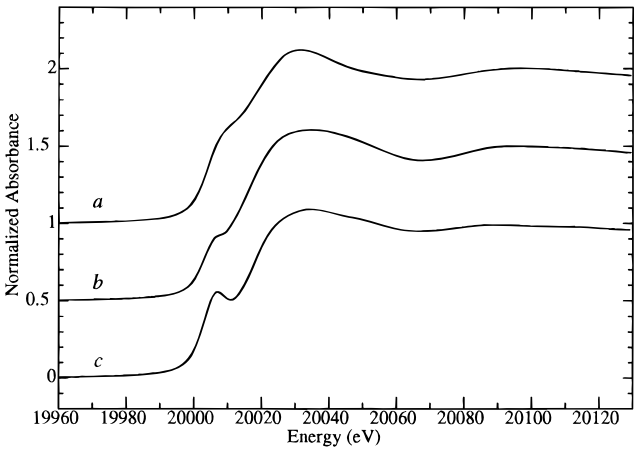

Figure 3. Mo K-edge X-ray absorption near-edge spectra of the three compounds (a) $Mo(N[R]Ar)_3$, (b) $(\mu\text{-}N_2)[Mo(N[R]Ar)_3]_2$, and (c) $NMo(N[R]Ar)_3$.

for the short core-hole lifetime of the molybdenum K-edge. For $Mo[N(R)Ar]_3$, a weak transition in the edge at about 20 007.0 eV, visible as a shoulder about halfway up the rising edge, is observed. For $(\mu\text{-}N_2)\{Mo[N(R)Ar]_3\}_2$, a more pronounced and lower-energy transition is seen at about 20 005.5 eV, and for $NMo[N(R)Ar]_3$, the most pronounced pre-edge feature is observed as a well-defined peak at 20 005.9 eV. The pre-edge feature in $(\mu\text{-}N_2)\{Mo[N(R)Ar]_3\}_2$ and $Mo[N(R)Ar]_3$ may be assigned to a 1s $\rightarrow$ 4d transition, which is formally dipole-forbidden and weakly quadrupole-allowed but gains intensity in a non-centrosymmetric molybdenum center by admixture of metal p-orbitals. This transition is analogous to the well-known "oxo-edge" feature of molybdenum enzymes, said to be characteristic of a species possessing terminal MoO groups.[28] The strong appearance of the 1s $\rightarrow$ 4d feature in the spectrum of $NMo[N(R)Ar]_3$ is highly consistent with the occurrence of a very short MoN triple bond. The intermediate appearance of the spectrum for $(\mu\text{-}N_2)\{Mo[N(R)Ar]_3\}_2$ is therefore consistent with an additional MoN bond somewhat longer than the triple bond of $NMo[N(R)Ar]_3$, but shorter than the MoN bonds to the N[R]Ar ligands.

Figure 4 (top) shows the k^3-weighted EXAFS of the three compounds and Figure 4 (bottom) the corresponding Fourier transforms. The data are of outstanding quality for all three compounds, extending out to $k = 21$ Å^{-1} for all spectra. The EXAFS of $Mo[N(R)Ar]_3$ and $NMo[N(R)Ar]_3$ are broadly similar in frequency; however, unlike $Mo[N(R)Ar]_3$, $NMo[N(R)Ar]_3$ exhibits a beat in its amplitude envelope which is maximal at around $k = 9$ Å^{-1} and again close to the end of the spectrum,

(28) Kutzler, F. W.; Natoli, C. R.; Misemer, D. K.; Doniach, S.; Hodgson, K. O. *J. Chem. Phys* **1980**, *73*, 3274.

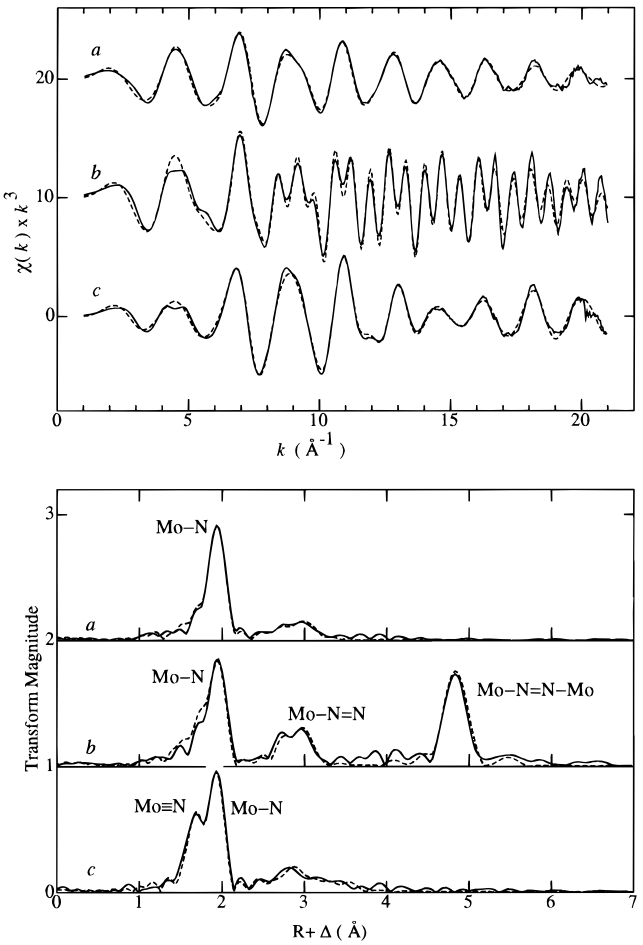

Figure 4. Mo K-edge EXAFS (upper panel) and EXAFS Fourier transforms (lower panel) of the three compounds (a) $Mo(N[R]Ar)_3$, (b) $(\mu\text{-}N_2)[Mo(N[R]Ar)_3]_2$, and (c) $NMo(N[R]Ar)_3$. The solid lines indicate data and the broken lines the best fits. The EXAFS is k^3-weighted raw data. The Fourier transforms have been phase-corrected using the first shell phase functions.

and minimal at around $k = 15$ Å^{-1}. Examination of the Fourier transforms shows that the origin of this beat is in the well-resolved split first shell of $NMo[N(R)Ar]_3$, which is observed to have an extra peak, fitted as a short MoN triple bond, to the low-*R* side of the N[R]Ar MoN peak. Both $Mo[N(R)Ar]_3$ and $NMo[N(R)Ar]_3$ also show low-amplitude scattering at around 3 Å which is attributable to Mo···C interactions. In marked contrast, the EXAFS spectrum of $(\mu\text{-}N_2)\{Mo[N(R)Ar]_3\}_2$ is dominated by high-frequency waves which persist to the end of the data. The Fourier transform exhibits an increase in amplitude (compared with $Mo[N(R)Ar]_3$ and $NMo[N(R)Ar]_3$) at around 3 Å, consistent with the presence of Mo···N backscattering, and a substantial peak at just below 5 Å, which is attributable to interactions involving Mo···Mo backscattering. The intensity of the peak, given its radial distance and coordination number (just 1), suggests that considerable enhancement from multiple scattering is likely in this outer-shell EXAFS.

The EXAFS total amplitude, phase-shift, and mean free path functions used in the curve-fitting were calculated using the program *feff* of Rehr and co-workers[29] (see Experimental Section for details). The results of EXAFS curve-fitting are shown as broken lines in Figure 4, and the corresponding numerical results of the curve-fitting are summarized in Table 2. Excellent correspondence between data and fit is found for all three compounds.

The final refined interatomic distances for the frozen solution of $Mo[N(R)Ar]_3$ were found to be in good agreement with the −86 °C crystal structure (see above), indicating that the molecule is not highly constrained by crystal packing forces. The refined interatomic distances to the ligands for the three compounds also show very little variation within the estimated errors, suggesting that their radial configuration is largely invariant. However, some slight spatial rotation or tilting of the ligands cannot be ruled out by EXAFS alone, although this is unlikely due to steric considerations.

The fit of the MoNNMo core of $(\mu\text{-}N_2)\{Mo[N(R)Ar]_3\}_2$ was found to be extremely sensitive to the Mo···Mo interatomic distance, which was always very close to 4.94 Å. The closer core distances were a little more difficult to determine due in part to correlations with ligand interactions. Therefore, it was decided to carry out search profiles to help determine both the linearity and the dinitrogen NN distance; Figure 5 shows the results of these searches. In the left-hand panel, the MoNN angle θ was varied, assuming a symmetrical molecule and a constant dinitrogen NN distance for both *cis* and *trans* geometric arrangements. New phase, amplitude, and mean free path functions were calculated for each point, and with fixed core distances, other parameters were refined to give the best fit. Figure 5 shows that the fit is very sensitive to θ and that the minimum in fit-error lies very close to 180° for both conformations. It is also interesting to note from this figure that the *cis* conformation is much more sensitive than the *trans* to θ; the small inset Fourier transforms show that for 170° *cis* the 5-Å peak has all but disappeared, whereas for 160° *trans* it is still substantial. This can be explained by examining the angular displacement (*i.e.*, the line of sight) of the MoN (dinitrogen) vectors with respect to the Mo···Mo vector which, for these interatomic distances and the closest MoN, is approximately 4 times greater for the *cis* arrangement for a given angle θ.[30] The right-hand graph shows the effect of varying the dinitrogen NN distance for a fixed Mo···Mo distance, assuming a linear molecule, and exhibits a very well-defined minimum at around 1.19 Å.

The final best fit for $(\mu\text{-}N_2)\{Mo[N(R)Ar]_3\}_2$ as shown in Table 2 and Figure 6 was found to be with a linear MoNNMo arrangement and a dinitrogen NN distance of 1.19(2) Å. As expected for such an arrangement and as calculated by *feff*,[29] substantial multiple scattering contributions to the outer coordination shells were necessary to account for these components. Figure 6 shows a deconvolution of all the paths contributing significantly to the EXAFS of $(\mu\text{-}N_2)\{Mo[N(R)Ar]_3\}_2$. The left-hand panel shows the data and fit at the top and then the individual waves contributing; the right-hand panel shows pictorially the corresponding scattering paths with respect to the molecule. Thus, the ligands contribute five unique waves (b−f), whereas the MoNNMo unit contributes one single-scattering wave (a) to the first shell, three unique waves to the 3-Å shell (one each 2-leg, 3-leg, and 4-leg paths, g−i) and 10 unique waves to the 5-Å shell (one 2-leg, two 3-leg, four 4-leg, two 5-leg, and one 6-leg paths, j−s). However, despite the numerous paths included in the refinement, only four new variables were required to fit the Mo···N and Mo···Mo outer shells of the MoNNMo unit because the parameters R and σ^2 for all single- and multiple-scattering paths of a given distance were floated as a common parameter.

(29) (a) Rehr, J. J.; Mustre de Leon, J.; Zabinsky, S. I.; Albers, R. C. *J. Am. Chem. Soc.* **1991**, *113*, 5135. (b) Mustre de Leon, J.; Rehr, J. J.; Zabinsky, S. I.; Albers, R. C. *Phys. Rev.* **1991**, *B44*, 4146.

(30) For *cis*, the displacement $\phi = 180 - \theta$, whereas for *trans*, $\sin\theta/R_{Mo-Mo} = \sin\phi/R_{N\equiv N}$.

Table 2. EXAFS Curve-Fitting Results[a]

		$Mo(N[R]Ar)_3$		$(\mu\text{-}N_2)[Mo(N[R]Ar)_3]_2$		$NMo(N[R]Ar)_3$	
interaction	*N*	*R*	σ^2	*R*	σ^2	*R*	σ^2
Mo≡N	1					1.655(2)	0.0014(2)
Mo−N	1[b]			1.876(5)	0.0019(1)[g]		
Mo−N	3	1.982(2)	0.0022(1)	1.983(2)	0.0021(1)[g]	1.975(2)	0.0020(1)
Mo···C_R	3	3.155(8)	0.0035(6)	3.153[h]	0.0071(18)	3.151(8)	0.0031(2)
Mo···C_{Ar1}	3	2.854(16)	0.0097(20)	2.838(19)	0.0052	2.862(7)	0.0035(5)
Mo···C_{Ar2}	3	3.29(4)	0.014(5)[d]	3.34[h]	0.015(11)[e]	3.38(2)	0.0064(15)[f]
Mo···C_{Ar6}	3	3.76(6)	0.014(5)[d]	3.71[h]	0.015(11)[e]	3.66(2)	0.0064(15)[f]
Mo···N	1[b]			3.069(12)	0.0026(9)		
Mo···Mo	1[b]			4.944(2)	0.0025(1)		
E_0		−12.2(6)		−13.1[h]		−13.9(9)	
error[c]		0.150		0.270		0.149	
T/K		200		10		10	

[a] Coordination number *N*, interatomic distance *R* (Å), Debye−Waller factor σ^2 (Å^2) and offset for $k = 0$, E_0 (eV). Three times the estimated standard deviations of floated parameters, obtained from the diagonal elements of the covariance matrix, are shown in parentheses after the values. [b] These coordination numbers were adjusted to account for 75% sample purity (see Experimental Section). [c] Error is given by $\Sigma[(\chi_{obsd} - \chi_{calcd})^2k^6]/\Sigma[\chi_{obsd}^2k^6]$. [d–f] Floated to be equal as a single parameter in the fit. [g] Floated with a constant ratio as a single parameter in the fit. [h] Value fixed at the mean of those of the starting material and the end product.

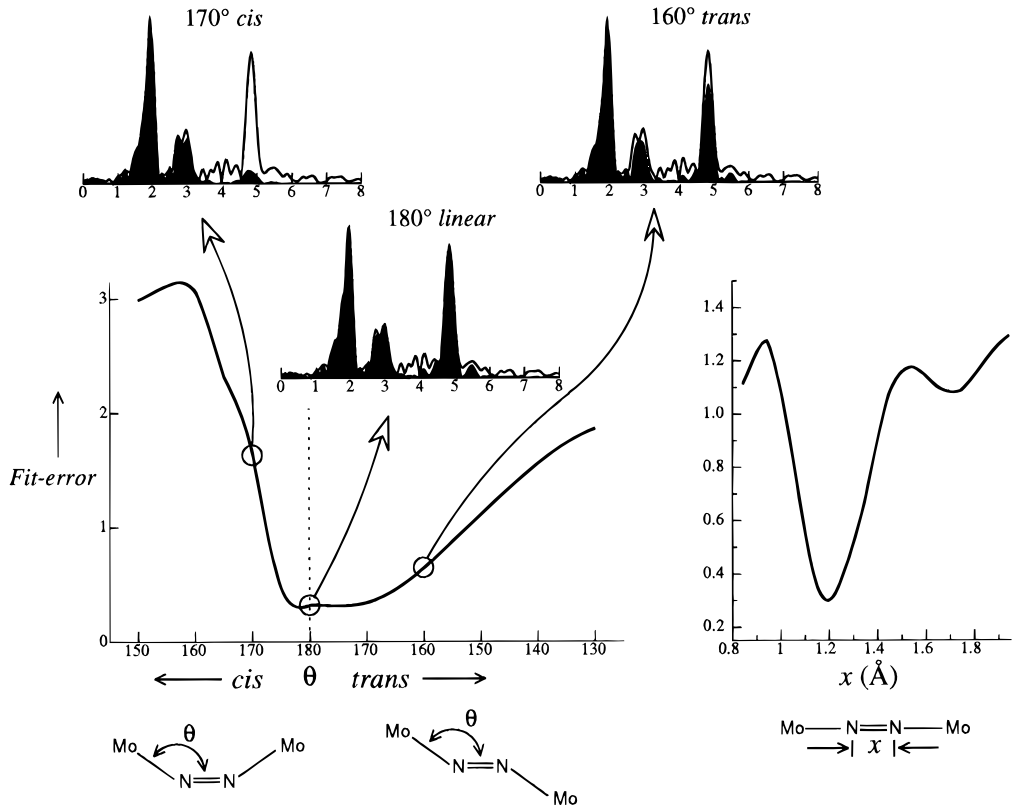

Figure 5. Search profiles for the linearity of the MoNNMo and for the NN distance of $(\mu\text{-}N_2)[Mo(N[R]Ar)_3]_2$, illustrating the sensitivity of the EXAFS fit to the core MoNNMo geometry. Both profiles were calculated using a fixed Mo···Mo distance of 4.94 Å. The geometry search profile (left plot) used a fixed NN distance of 1.19(2) Å, and the NN distance search profile (right plot) assumed a linear MoNNMo arrangement. The other parameters were refined to obtain the best fits possible. The fit-error in this case is given by $\Sigma[(\chi_{obsd} - \chi_{calcd})^2k^6]/n$, where *n* is the number of data points. The inset Fourier transforms show the fit (filled curve) superimposed on the data (line).

(v) Molecular and Electronic Structure of $(\mu\text{-}N_2)\{Mo[N(R)Ar]_3\}_2$. According to the EXAFS and NMR data (*vide supra*), and consistent with the Raman and magnetic data (*vide infra*), $(\mu\text{-}N_2)\{Mo[N(R)Ar]_3\}_2$ is formulated as a symmetrical bridging dinitrogen complex[9] with a roughly linear MoNNMo core. Bimetallic complexes with side-on or end-on bridging dinitrogen ligands have been the subject of theoretical studies.[31] The best precedent for our proposed structure is $(\mu\text{-}N_2)[Mo\{R'NCH_2CH_2\}_3N]_2$ ($R' = t\text{-}BuMe_2Si$),[9z] which contains molybdenum in the same formal oxidation state as for $(\mu\text{-}N_2)\{Mo[N(R)Ar]_3\}_2$, and which is likewise ligated by amido groups. A point of disparity between the two complexes is the coordination number 5 at Mo in the former compared with 4 in the latter. A second point of distinction between the two complexes is the presence of marginally less electron-releasing silylated amido substituents in the former. A third, rather intriguing point of distinction between these two closely related dinitrogen complexes is that $(\mu\text{-}N_2)[Mo\{R'NCH_2CH_2\}_3N]_2$ has not been reported to undergo thermal NN bond cleavage. It has been predicted, on theoretical grounds, that such an NN bond cleavage reaction for $(\mu\text{-}N_2)[Mo\{R'NCH_2CH_2\}_3N]_2$ would

(31) Blomberg, M. R. A.; Siegbahn, P. E. M. *J. Am. Chem. Soc.* **1993**, *115*, 6908. Tatsumi, K.; Hoffmann, R. *J. Am. Chem. Soc.* **1981**, *103*, 3328. See also ref 9f above.

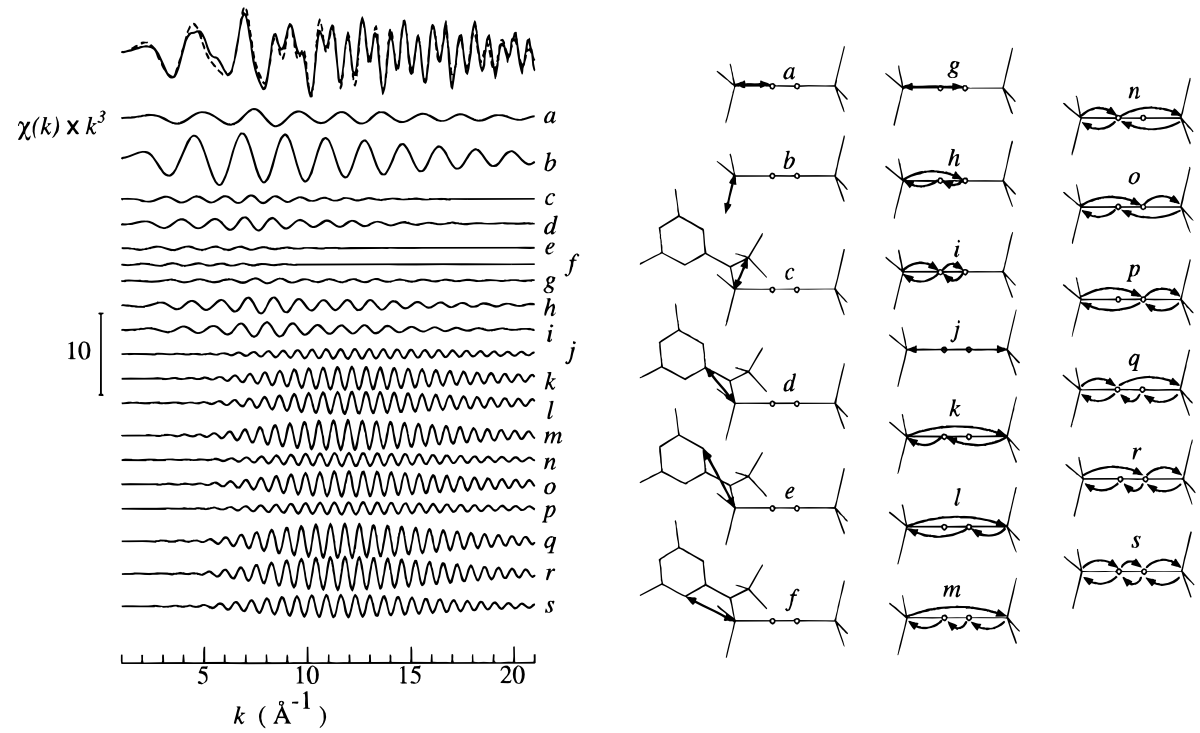

Figure 6. Scattering interactions contributing to the EXAFS of (μ-N_2)[Mo(N[R]Ar)$_3$]$_2$. The left plot shows the experimental data and fit (solid and broken lines, respectively, at top) and the deconvolution of the individual scattering interactions contributing to the total EXAFS. The right picture shows, for each of the waves at the left, the corresponding scattering paths in the molecule. Note that paths b−f have a 3-fold degeneracy due to the geometry of the ligands and paths h, k−m, o, q, and r are 2-fold degenerate because the reverse scattering path also contributes.

be an uphill process.[5] On the other hand, note that the nitrido complex NMo(MeNCH$_2$CH$_2$)$_3$N is known[32] and has not been reported to dimerize.[33]

It is instructive to compare the important metrical parameters for (μ-N_2){Mo[N(R)Ar]$_3$}$_2$ with the literature values for (μ-N_2)[Mo{R′NCH$_2$CH$_2$}$_3$N]$_2$; these are, respectively, as follows (Å): d(NN) = 1.19(2), 1.20(2); d(Mo−N_2) = 1.876(5), 1.907(8); and d(Mo−NRR′) = 1.983(2), 2.01(1). An NN bond order slightly greater than 2 is indicated for both molecules according to the observed d(NN) values; we elaborate upon this issue in the section devoted to Raman data (*vide infra*). In addition, both complexes are intensely purple and paramagnetic. The slightly longer Mo−NRR′ values for the silylated compound can be attributed either to its higher coordination number or to a somewhat reduced electron-donor capacity of silylated amido ligands as compared with the N[R]Ar ligand. Some support for the latter interpretation rests on the observation of a significantly shorter d(Mo−N_2) for (μ-N_2){Mo[N(R)Ar]$_3$}$_2$, indicative of greater dπ → pπ* back-donation in this case.

Molecules possessing linear MNNM moieties have been the subject of several molecular orbital studies in the past.[31] The analysis given by Bercaw and co-workers is particularly lucid.[9f] Four doubly-degenerate levels comprise the MNNM π-system. In the point group S_6, to which (μ-N_2){Mo[N(R)Ar]$_3$}$_2$ likely belongs,[34] these levels bear the Mulliken labels 1e$_u$ (NN π), 1e$_g$ (MoN π, NN π*), 2e$_u$ (Mo nonbonding), and 2e$_g$ (MoN π* and NN π*) and have the indicated characters (see Figure 7, left). The 1e$_u$ and 2e$_u$ levels are localized primarily on the N_2 and the Mo centers, respectively, due to the substantial energy mismatch between them.[35] Because the molybdenum π-donor orbitals are energetically well matched with the NN π* levels, the 1e$_g$ and 2e$_g$ levels to which they give rise are quite delocalized. Ten electrons are available for population of the four doubly degenerate levels in (μ-N_2){Mo[N(R)Ar]$_3$}$_2$, leading to the expected configuration (1e$_u$)^4(1e$_g$)^4(2e$_u$)^2(2e$_g$)^0. Such a configuration is reasonable for an isolable molecule since the doubly-degenerate HOMO is nonbonding and molybdenum-based, while the LUMO is everywhere antibonding. Furthermore, this configuration demands that the molecule be paramagnetic, with two unpaired electrons. Experimental confirmation of the latter prediction was achieved through SQUID magnetometry studies carried out on (μ-N_2){Mo[N(*t*-Bu)Ph]$_3$}$_2$, of which relatively pure powder samples could be obtained. The data fit the Curie−Weiss law with good agreement in the temperature range 29−300 K with μ = 2.85 μ_B (Figure 8), consistent with the presence of two unpaired electrons. A further issue of interest in the context of the electronic structure of (μ-N_2){Mo[N(R)Ar]$_3$}$_2$ is the origin of its purple color. While it is tempting to ascribe the intense 547-nm band to a (2e$_u$)^2(2e$_g$)^0 → (2e$_u$)^1(2e$_g$)^1 transition having π → π* character, Bercaw and co-workers have pointed out that metal-to-metal charge transfer bands could be important for systems of this type.[9f]

(vi) Raman Spectra of (μ-N_2){Mo[N(R)Ar]$_3$}$_2$ and (μ-$^{15}N_2$){Mo[N(R)Ar]$_3$}$_2$. Since a symmetrical linear structure for (μ-N_2){Mo[N(R)Ar]$_3$}$_2$ is indicated by the EXAFS data described above, the Raman spectrum of this species was recorded to garner additional information concerning the NN bond length and order. Spectra of (μ-N_2){Mo[N(R)Ar]$_3$}$_2$ and (μ-$^{15}N_2$){Mo[N(R)Ar]$_3$}$_2$ are displayed in Figure 9. Each complex exhibits one strong Raman band attributable to ν(NN) in the observation window, located at 1630 cm^{-1} for (μ-N_2){Mo[N(R)Ar]$_3$}$_2$ and

(32) Plass, W.; Verkade, J. G. *J. Am. Chem. Soc.* **1992**, *114*, 2275.

(33) An example of μ-N_2 bridge formation via coupling of terminal nitrido ligands has been reported: Buhr, J. D.; Taube, H. *Inorg. Chem.* **1979**, *18*, 2208. Lam, H.-W.; Che, C.-M.; Wong, K.-Y. *J. Chem. Soc., Dalton Trans.* **1992**, 1411. See also ref 9ll above.

(34) The related molecule (μ-P)[Mo(^{t}BuNPh)$_3$]$_2$ (C_i) nearly belongs to the point group S_6 according to a single-crystal X-ray diffraction study: Johnson, M. J. A.; Odom, A. L.; Cummins, C. C. Manuscript submitted elsewhere.

(35) This qualitative notion is supported by extended Hückel calculations carried out using the CAChe system.

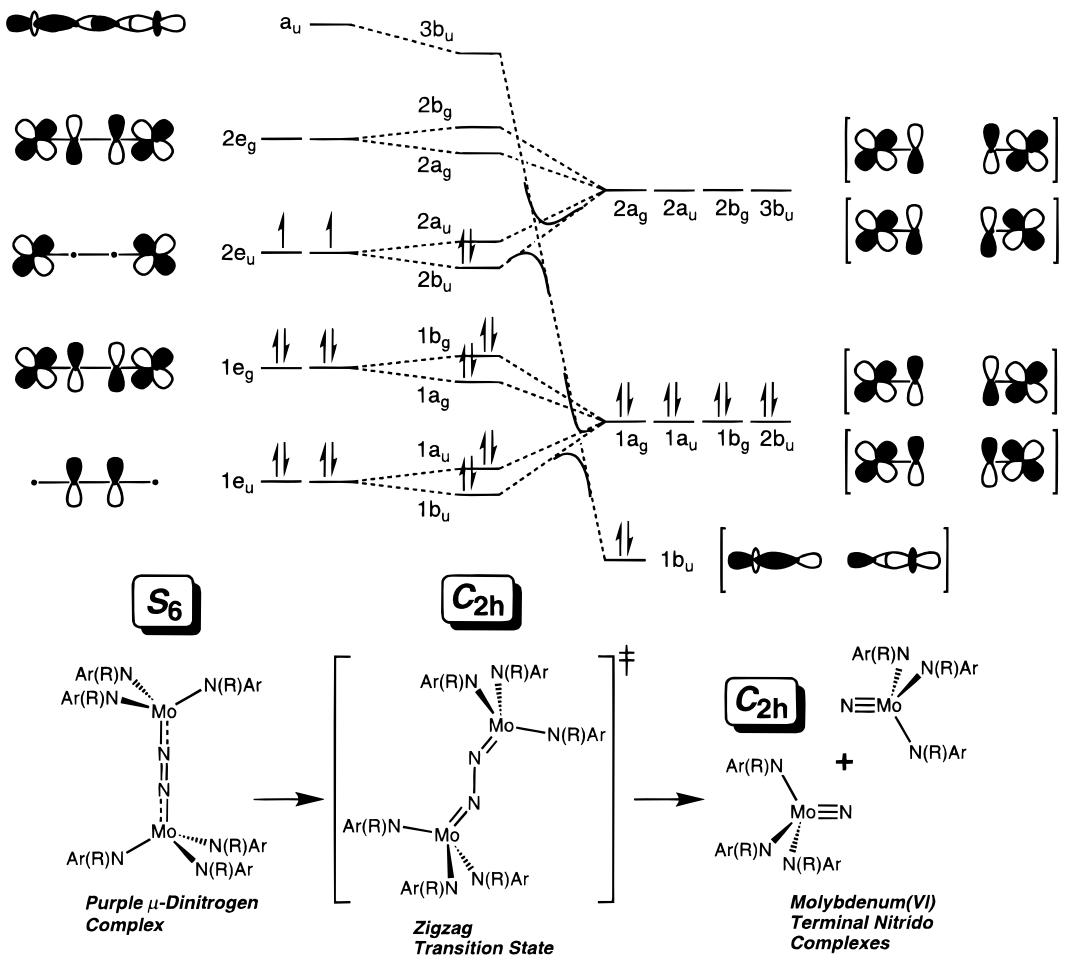

Figure 7. Qualitative molecular orbital correlation diagram for the conversion of S_6 $(\mu\text{-}N_2)[Mo(N[R]Ar)_3]_2$ to 2 $NMo(N[R]Ar)_3$ (C_{2h}) via a C_{2h} transition state. Only the most important σ and π levels of the MoNNMo core are depicted. The numbering scheme for the energy levels takes into account only those orbitals that are pictured.

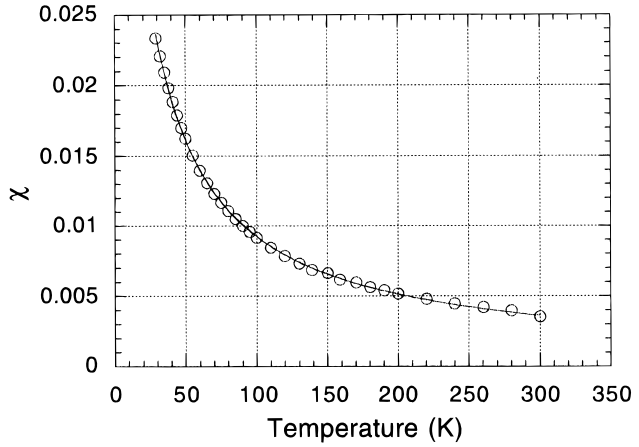

Figure 8. SQUID magnetic susceptibility data for $(\mu\text{-}N_2)[Mo(N[t\text{-}Bu]Ph)_3]_2$ from 29 to 300 K fit to the Curie−Weiss law (see Experimental Section for details). The fit yields $\mu = 2.85\ \mu_B$.

at 1577 cm^{-1} for its doubly-labeled isotopomer (calcd 1575 cm^{-1}). These data are compared with those for other NN-containing molecules in Figure 10,[36] which correlates $[d(NN)]^{3/2}$ with ν(NN) according to Fryzuk, Loehr, and co-workers.[9h] The best-fit line ($R = 0.94$) in Figure 10 follows the equation $\nu(NN) = -1840[d(NN)]^{3/2} + 4130$, leading to a prediction of ca. 1.23 Å for the d(NN) of $(\mu\text{-}N_2)\{Mo[N(R)Ar]_3\}_2$. Agreement between the latter number and that obtained by EXAFS [1.19(2) Å, *vide supra*] is fairly good despite the rough nature of the correlation. An NN bond order of approximately 2 for $(\mu\text{-}N_2)\{Mo[N(R)Ar]_3\}_2$ is indicated by comparison of its ν(NN) and d(NN) with those for the other NN-containing molecules in Figure 10.

(vii) Activation Parameters for NN Bond Cleavage and Comments on the Transition State. Conversion of purple $(\mu\text{-}N_2)\{Mo[N(R)Ar]_3\}_2$ to 2 equiv of the nitrido complex $NMo[N(R)Ar]_3$ is conveniently monitored by following the decay of an intense 547-nm band. The product nitrido complex exhibits negligible absorbance at this wavelength. Clean, reproducible first-order kinetic behavior over ca. 4 half-lives was observed for both $(\mu\text{-}N_2)\{Mo[N(R)Ar]_3\}_2$ and $(\mu\text{-}^{15}N_2)\{Mo[N(R)Ar]_3\}_2$ over the temperature range 25−65 °C. Multiple (three to six) rate constant determinations were performed at 2.5 °C intervals over this range. Averages of the observed rate constants for breakup of $(\mu\text{-}N_2)\{Mo[N(R)Ar]_3\}_2$ are plotted against temperature in Figure 11, where the solid curve represents the best fit to the exponential form of the Eyring

(36) (a) Hydrazine d(NN) = 1.46 Å: Collin, R. L.; Lipscomb, W. N. *Acta Crystallogr.* **1951**, *4*, 10. (b) hydrazine ν(NN) = 938 cm^{-1}: Durig, J. R.; Bush, S. F.; Mercer, E. E. *J. Chem. Phys.* **1966**, *44*, 4238. (c) $(PMe_2Ph)_4ClRe(\mu\text{-}N_2)MoCl_4(OMe)$ d(NN) = 1.21 Å, ν(NN) = 1660 cm^{-1}: ref 9tt above. (d) Azobenzene ν(NN) = 1440 cm^{-1}: Hacker, H. *Spectrochim. Acta* **1965**, *21*, 1989. (e) Azobenzene d(NN) = 1.248(3) Å: Bouwstra, J. A.; Schouten, A.; Kroon, A.; Helmholdt, R. B. *Acta Crystallogr.* **1985**, *C41*, 420. (f) *trans*-Diazene d(NN) = 1.252 Å: Whitelegg, D.; Woolley, R. G. *THEOCHEM* **1990**, *68*, 23. (g) *trans*-Diazene ν(NN) = 1541 cm^{-1}: Ackerman, M. N.; Burdge, J. J.; Craig, N. C. *J. Chem. Phys.* **1973**, *58*, 215. (h) $(\mu\text{-}N_2)[ZrCp^*_2(N_2)]_2$ d(NN) = 1.182(5) Å, ν(NN) = 1578 cm^{-1}: ref 9f above. (i) $(\mu\text{-}N_2)[CpZrN(SiMe_2CH_2P^iPr_2)_2]_2$ d(NN) = 1.301(3) Å, ν(NN) = 1211 cm^{-1} and $(\mu\text{-}N_2)[ClZrN(SiMe_2CH_2P^iPr_2)_2]_2$ d(NN) = 1.548(7) Å, ν(NN) = 731 cm^{-1}: ref 9h above. (j) $(\mu\text{-}N_2)[Ru(NH_3)_5]_2^{4+}$ d(NN) = 1.124(15) Å, ν(NN) = 2100 cm^{-1}: Treitel, I. M.; Flood, M. T.; Marsh, R. E.; Gray, H. B. *J. Am. Chem. Soc.* **1969**, *91*, 6512.

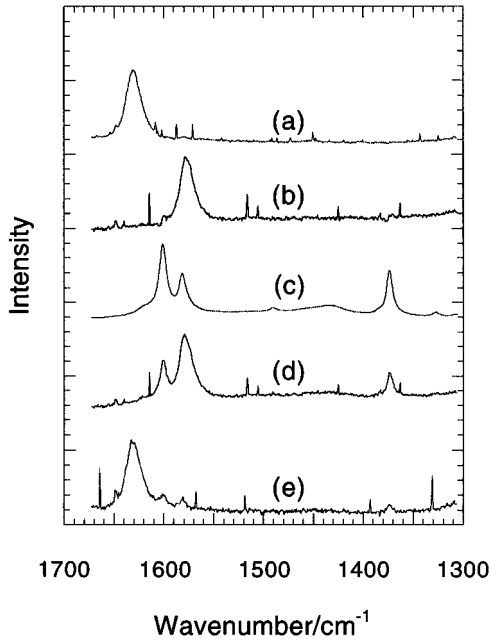

Figure 9. (a) Resonance Raman (RR) spectrum of (μ-N_2)[Mo(N[R]-Ar)$_3$]$_2$ as a solution in toluene with toluene spectrum digitally subtracted; ν(NN) = 1630 cm^{-1}. (b) RR spectrum of (μ-$^{15}N_2$)[Mo(N[R]Ar)$_3$]$_2$ as a solution in toluene with toluene spectrum digitally subtracted; $\nu(^{15}N^{15}N)$ = 1577 cm^{-1} (calcd 1575 cm^{-1}). (c) Raman spectrum of toluene solvent. (d) Raw RR spectrum of (μ-$^{15}N_2$)[Mo(N[R]Ar)$_3$]$_2$ in toluene with no subtraction of solvent spectrum. (e) Raw RR spectrum of (μ-N_2)[Mo(N[R]Ar)$_3$]$_2$ in toluene with no subtraction of solvent spectrum.

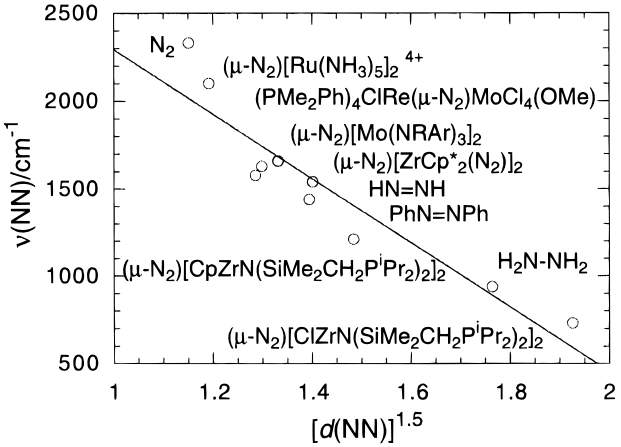

Figure 10. Plot of $[d(\mathrm{NN})]^{3/2}$ versus ν(NN) for a number of NN-containing molecules. See text for more information.

equation. The corresponding data for (μ-$^{15}N_2$){Mo[N(R)Ar]$_3$}$_2$ are presented in Figure 12. See the Experimental Section for details of the data collection and analysis. Activation parameters obtained from the fit are as follows: $\Delta H^{\ddagger}$ = 23.3 ± 0.3 kcal·mol^{-1} and $\Delta S^{\ddagger}$ = 2.9 ± 0.8 cal·mol^{-1}·K^{-1}. Morokuma and co-workers recently calculated an activation energy of 21 kcal·mol^{-1} for hypothetical (μ-N_2)[Mo(NH$_2$)$_3$]$_2$.[5] The agreement with our experimental value is manifest.

Morokuma and co-workers have suggested that the lowest-energy transition state for a corresponding NN cleavage process involving hypothetical (μ-N_2)[Mo(NH$_2$)$_3$]$_2$ would involve a zigzag (C_{2h}) transition structure (TS) with an elongated NN bond (1.544 Å, bond order of ca. 1) and shortened Mo−N_2 bonds (1.759 Å).[5] Such a TS is consistent with our activation parameters and is characterized by a significant degree of NN bond cleavage. A zigzag-shaped TS is eminently plausible in

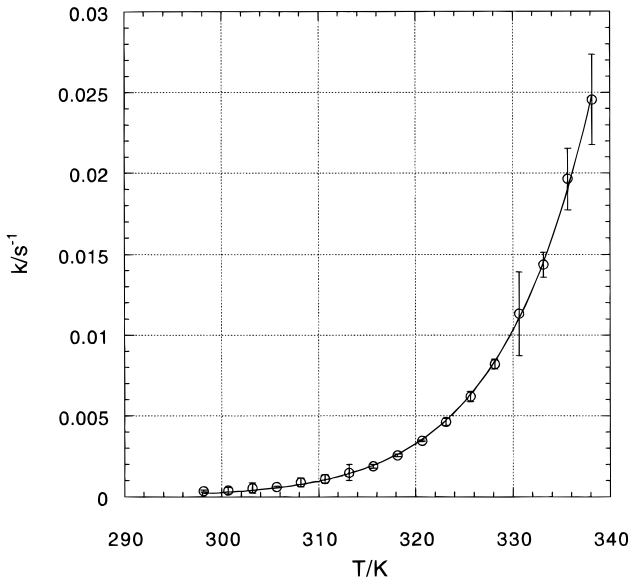

Figure 11. Exponential least-squares fit of first-order rate constants (k) versus temperature (T) to the Eyring equation $k = (k_B T/h)\exp(\Delta S^{\ddagger}/R)\exp(-\Delta H^{\ddagger}/RT)$ for the reaction (μ-N_2)[Mo(N[R]Ar)$_3$]$_2$ → 2 NMo(N[R]Ar)$_3$. Activation parameters obtained from the fit are $\Delta H^{\ddagger}$ = 23.3 ± 0.3 kcal·mol^{-1} and $\Delta S^{\ddagger}$ = 2.8 ± 1.1 cal·mol^{-1}·K^{-1}.

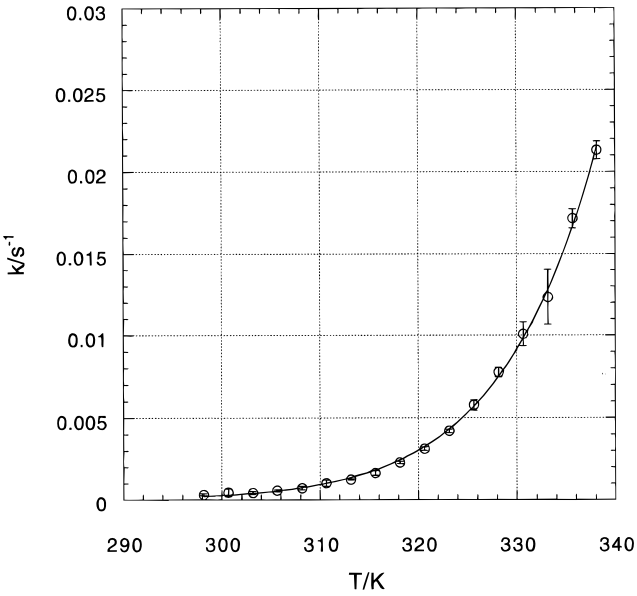

Figure 12. Exponential least-squares fit of first-order rate constants (k) versus temperature (T) to the Eyring equation $k = (k_B T/h)\exp(\Delta S^{\ddagger}/R)\exp(-\Delta H^{\ddagger}/RT)$ for the reaction (μ-$^{15}N_2$)[Mo(N[R]Ar)$_3$]$_2$ → 2 ^{15}NMo(N[R]Ar)$_3$. Activation parameters obtained from the fit are $\Delta H^{\ddagger}$ = 22.6 ± 0.3 kcal·mol^{-1} and $\Delta S^{\ddagger}$ = 0.4 ± 1.1 cal·mol^{-1}·K^{-1}.

view of the electronic structure of (μ-N_2){Mo[N(R)Ar]$_3$}$_2$ as described above. In particular, while (μ-N_2){Mo[N(R)Ar]$_3$}$_2$ possesses 10 π electrons and six σ electrons in its MoNNMo framework, two NMo[N(R)Ar]$_3$ molecules together require eight π and eight σ electrons for their nitrido linkages. During NN cleavage, then, two electrons must pair and pass from the MoNNMo π-system to the MoN···NMo σ-system. A C_{2h} TS provides a mechanism for this in that the decreased symmetry renders nondegenerate the two Mo-based nonbonding orbitals originating from the $2e_u$ level of ground-state (μ-N_2){Mo[N(R)-Ar]$_3$}$_2$ (see Figure 7, a qualitative molecular orbital correlation diagram for the process). Furthermore, one of these orbitals ($2b_u$) lies in the MoNNMo plane of the C_{2h} TS and is of appropriate symmetry to correlate, via avoided crossings, with

the σ symmetry orbital (designated $1b_u$) that is doubly occupied in the products but high in energy and unoccupied in linear $(\mu\text{-}N_2)\{Mo[N(R)Ar]_3\}_2$. Any postulated mechanism for simple dissociation of $(\mu\text{-}N_2)\{Mo[N(R)Ar]_3\}_2$ should encompass these essential symmetry considerations. NN bond cleavage along a linear trajectory is symmetry forbidden. The postulate of a C_{2h} TS is reasonable on electronic grounds, but importantly, it is also reasonable on steric grounds. Whereas the two Mo centers are separated by 4.944(2) Å in linear $(\mu\text{-}N_2)\{Mo[N(R)Ar]_3\}_2$ (*vide supra*), the intermolybdenum separation in the bent TS calculated for $(\mu\text{-}N_2)[Mo(NH_2)_3]_2$ is ca. 4.81 Å. There exists independent evidence that two $Mo[N(R)Ar]_3$ moieties can accommodate an intermolybdenum separation of 4.49 Å with a single-atom bridge.[34] Therefore, the calculated C_{2h} TS cannot be construed to pose an insurmountable steric problem.

(viii) The $^{15}N_2$ Isotope Effect for NN Bond Cleavage. Based on assumptions of (i) a linear transition state, (ii) the attribution of observed rate differences solely to zero-point energy differences in the isotopomers, and (iii) a diatomic system, primary kinetic isotope effects (KIEs) may be calculated from $k_1/k_2 = \exp[(hc/2k_BT)(\nu_1-\nu_2)]$.[37] In the case of dinitrogen itself, the value of ν_1 is 2329.9 cm^{-1} (from the Raman spectrum of $^{14}N_2$), and the value of ν_2 is 2252.1 cm^{-1} (from the Raman spectrum of $^{15}N_2$).[38] Because the force constant (k_f) is dependent only on electronic factors and is therefore the same for $^{14}N_2$ as for $^{15}N_2$,[39] and given that the reduced masses μ_1 and μ_2 for $^{14}N_2$ and $^{15}N_2$ are ca. 7.0 and 7.5, respectively,[40] the classical harmonic relationship for these isotopomers is $1.035\nu_2 = \nu_1$, in close agreement with the experimental value. The theoretical KIE, $k(^{14}N_2)/k(^{15}N_2)$, for thermal dissociation of dinitrogen to two N atoms is 1.21 at 298 K and 1.18 at 338 K. As another example, consider a typical symmetrical alkyl diazo compound RN═NR having an NN stretching frequency (ν_1) of ca. 1575 cm^{-1};[41] the calculated ν_2 for $R^{15}N{=}{}^{15}NR$ is 1522 cm^{-1}, so the theoretical KIE for dissociation to two alkylnitrene moieties is 1.14 at 298 K and 1.12 at 338 K. The two preceding examples, with their attendant assumptions, permit the following prediction concerning a primary KIE for scission of an NN double-to-triple bond: $k(^{14}N_2)/k(^{15}N_2)$ should be somewhere between 1.12 and 1.21 and will be essentially invariant over the temperature range 298−338 K, the temperature range employed in our kinetic study. The observed temperature dependence of the isotope effect for scission of $(\mu\text{-}N_2)\{Mo[N(R)Ar]_3\}_2$ to 2 $Mo[N(R)Ar]_3$ can be fitted to the equation $k_1/k_2 = \exp[(hc/2k_BT)(\nu_1-\nu_2)]$ to yield a prediction for $\nu_1 - \nu_2$; such a fit is displayed in Figure 13. The fit yields a prediction for $\nu_1 - \nu_2$ of 52 ± 9 cm^{-1}, which is (perhaps fortuitously) very close to the observed value of 53 cm^{-1} obtained (*vide supra*) by Raman spectroscopy for $(\mu\text{-}N_2)\{Mo[N(R)Ar]_3\}_2$ and $(\mu\text{-}^{15}N_2)\{Mo[N(R)Ar]_3\}_2$. Within the confines of the present simplistic analysis, the observed isotope effect is of the expected magnitude for rate-determining NN bond cleavage.[42] A more sophisticated analysis would take into account such effects as possible nuclear spin contributions to the isotope effect,[43] and coupling of the NN vibrational mode with other fundamental modes of the $(\mu\text{-}N_2)\{Mo[N(R)Ar]_3\}_2$ molecule.[44] $^{15}N_2$ isotope effects have evidently not been observed for N_2 cleavage by nitrogenase enzymes, where decomplexation of oxidized Fe protein from the FeMo protein is thought to be rate-limiting.[45]

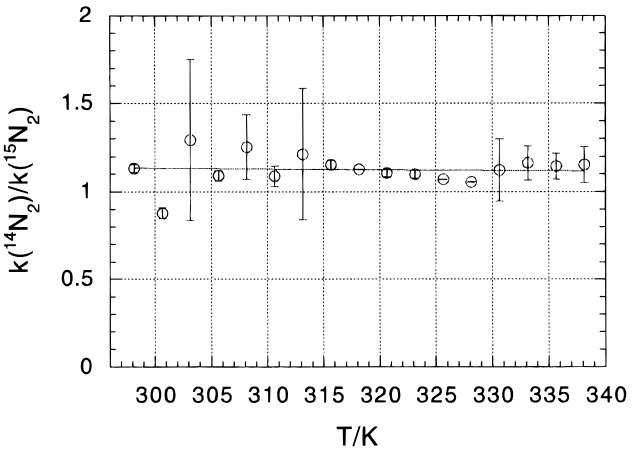

Figure 13. Plot of rate constant ratios for the reactions $(\mu\text{-}N_2)[Mo(N[R]Ar)_3]_2 \rightarrow 2\ NMo(N[R]Ar)_3$ and $(\mu\text{-}^{15}N_2)[Mo(N[R]Ar)_3]_2 \rightarrow 2\ ^{15}NMo(N[R]Ar)_3$. The unweighted least-squares fit is to the equation $k_1/k_2 = \exp[(hc/2k_BT)(\nu_1-\nu_2)]$, see text, with $\nu_1 - \nu_2$ as the sole parameter. Given the attendant assumptions, the fit yields the prediction that the Raman NN stretching frequency for $(\mu\text{-}N_2)[Mo(N[R]Ar)_3]_2$ should lie 52 ± 9 cm^{-1} higher in energy than that for $(\mu\text{-}^{15}N_2)[Mo(N[R]Ar)_3]_2$.

(ix) X-ray Structure of NMo[N(*t*-Bu)Ph]$_3$. The new nitrido complex $NMo[N(t\text{-}Bu)Ph]_3$ is included in the present work in part because it was possible to characterize this compound structurally by single-crystal X-ray diffraction, whereas we have been unable to obtain suitable crystals of $NMo[N(R)Ar]_3$ for such a study. From a chemical standpoint the two systems are equivalent in every important respect, and it stands to reason that the solid-state structure of the latter should resemble closely that of the former. We have suggested that $NMo[N(R)Ar]_3$ is a monomeric, pseudotetrahedral species possessed of a short NMo triple bond, consistent with its ν(MoN) of 1042 cm^{-1}. The known,[46] crystallographically-characterized molecule $NMo(NPh_2)_3$ exhibits such features and served as close precedent, buttressing our assertions concerning the structure of $NMo[N(R)Ar]_3$. Related molybdenum nitrido complexes include $NMo(O^tBu)_3$,[47] $NMo(2,4,6\text{-}C_6H_2Me_3)_3$,[48] and $NMo(CH_2{}^tBu)_3$.[49] The X-ray structure of $NMo[N(t\text{-}Bu)Ph]_3$ presented no surprises (Figure 14; see Experimental Section for a complete list of bond lengths and angles). The molecule exhibits crystallographic 3-fold symmetry (point group C_3), with MoN bond lengths of 1.658(5) and 1.979(2) Å to the nitrido and amido nitrogens,

(37) Collecting the fundamental constants together leads to a user-friendly form of the equation: $k_1/k_2 = \exp(0.7193916\{\nu_1 - \nu_2\}/T)$. This equation leads to the familiar value for k_H/k_D of 6.9 at 298 K taking ν_1 and ν_2 as 2900 and 2100 cm^{-1}, respectively, for the breaking of a CH versus a CD bond. Westheimer, F. H. *Chem. Rev.* **1961**, *61*, 265. Carpenter, B. K. *Determination of Organic Reaction Mechanisms*; Wiley: New York, 1984.

(38) Bendtsen, J. *J. Raman Spectrosc.* **1974**, *2*, 133. Gilson, T. R.; Beattie, I. R.; Black, J. D.; Greenhalgh, D. A.; Jenny, S. N. *J. Raman Spectrosc.* **1980**, *9*, 361. From these references, the experimentally-determined vibrational frequency for $^{14}N^{15}N$ is 2291.3 cm^{-1}.

(39) Herzberg, G. *Molecular Spectra and Molecular Structure*; D. Van Nostrand: New York, 1945.

(40) Calculated using masses for ^{14}N and ^{15}N found in the following: Weast, R. C. *CRC Handbook of Chemistry and Physics*, 66th ed.; Weast, R. C., Ed.; CRC Press: Boca Raton, 1985.

(41) Dean, J. A. *Lange's Handbook of Chemistry*, 14th ed.; McGraw-Hill: New York, 1992.

(42) For isotope effects associated with O−O bond cleavage in acyl peroxides, see: Goldstein, M. J. *Science* **1966**, *154*, 1616. Goldstein, M. J.; Judson, H. A. *J. Am. Chem. Soc.* **1970**, *92*, 4122.

(43) Turro, N. J.; Kraeutler, B. *Acc. Chem. Res.* **1980**, *13*, 369.

(44) For an elegant "whole-molecule" deuterium equilibrium isotope effect study on the binding of ethylene to a transition metal complex, see: Bender, B. R. *J. Am. Chem. Soc.* **1995**, *117*, 11239.

(45) Thorneley, R. N. F.; Lowe, D. J. *Biochem. J.* **1983**, *215*, 393.

(46) Gebeyehu, Z.; Weller, F.; Neumüller, B.; Dehnicke, K. *Z. Anorg. Allg. Chem.* **1991**, *593*, 99.

(47) Chan, D. M.-T.; Chisholm, M. H.; Folting, K.; Huffman, J. C.; Marchant, N. S. *Inorg. Chem.* **1986**, *25*, 4170.

(48) Caulton, K. G.; Chisholm, M. H.; Doherty, S.; Folting, K. *Organometallics* **1995**, *14*, 2585.

(49) Herrmann, W. A.; Bogdanovic, S.; Poli, R.; Priermeier, T. *J. Am. Chem. Soc.* **1994**, *116*, 4989.

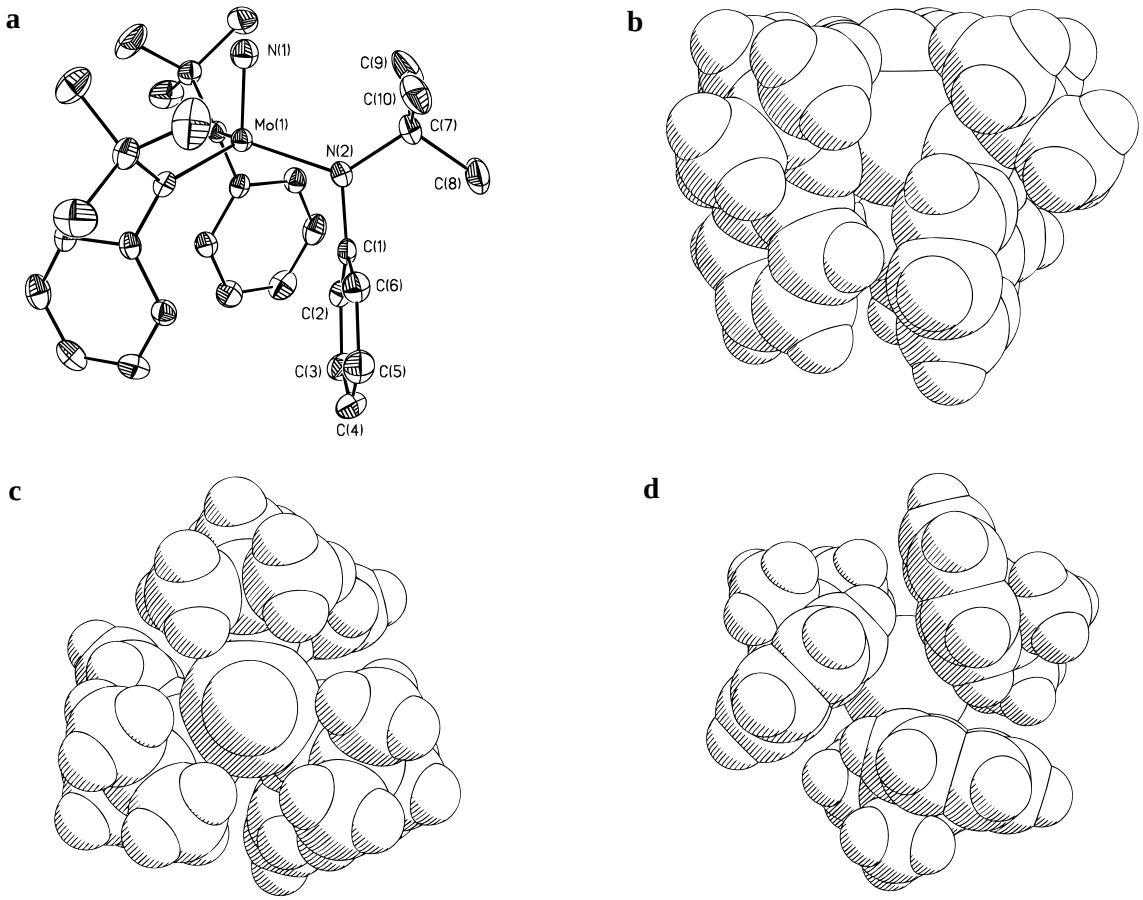

Figure 14. (a) Structural diagram and atom-labeling scheme for NMo(N[*t*-Bu]Ph)$_3$. Thermal ellipsoids are at the 35% probability level. Selected bond lengths (Å) and angles (deg) for NMo(N[*t*-Bu]Ph)$_3$ are as follows: Mo(1)−N(1), 1.658(5); Mo(1)−N(2), 1.979(2); C(1)−N(2), 1.444(4); N(2)−C(7), 1.513(3); N(1)−Mo(1)−N(2), 102.94(7); N(2)−Mo(1)−N(2)′, 115.13(5); C(1)−N(2)−C(7), 117.3(2); C(1)−N(2)−Mo(1), 113.5(2); C(7)−N(2)−Mo(1), 128.2(2). Space-filling representations of NMo(N[*t*-Bu]Ph)$_3$ viewed (b) perpendicular to the nitrido bond axis, (c) along the nitrido bond axis facing the hemisphere protected by *tert*-butyl groups, and (d) along the nitrido bond axis facing the hemisphere protected by phenyl groups.

respectively. These values are in excellent agreement with those determined by EXAFS for NMo[N(R)Ar]$_3$ (*vide supra*), namely, 1.655(2) and 1.975(2) Å, and also compare reasonably well with those calculated for hypothetical NMo(NH$_2$)$_3$,[5] namely, 1.678 and 1.966 Å. It is noteworthy that the geometry of the Mo[N(*t*-Bu)Ph]$_3$ fragment differs little from that in the starting Mo[N(R)Ar]$_3$ (*vide supra*) and Mo[N(*t*-Bu)Ph]$_3$ molecules, grossly speaking. Space-filling models (Figure 14b−d) reveal that the major difference is that the channel bounded by *tert*-butyl groups (Figure 14c) has expanded somewhat to accommodate the introduction of a nitrogen atom. The channel bounded by aryl residues, on the other hemisphere of the molecule, is constricted commensurately (Figure 14d). No short Mo···NMo contacts of the kind observed for solid-state NMo(O^{t}Bu)$_3$, a "shish kebab" polymer,[47] were found for NMo[N(*t*-Bu)Ph]$_3$. Indeed, none should be expected in view of the substantially greater steric demands of N[*t*-Bu]Ph or N[R]Ar as compared with *tert*-butoxide. A growing list of pseudo-C_3-symmetric, monomeric, structurally characterized complexes related to NMo[N(*t*-Bu)Ph]$_3$ includes PMo[N(R)Ar]$_3$,[2] PMo[N(*t*-Bu)Ph]$_3$,[50] ClTi[N(R)Ar]$_3$,[51] ITi[N(*t*-Bu)Ph]$_3$,[17] MeSn[N(R)Ar]$_3$, and ISn[N(R)Ar]$_3$.[22] C_3 symmetry thus represents a pervasive motif for complexes built with three *N*-*tert*-butylarylamido ligands and a single apical atom. The related chromium nitrido complexes NCr(N^{i}Pr$_2$)$_3$[52] and NCr(N^{i}Pr$_2$)$_2$(CH$_2$SiMe$_2$Ph)[53] are likewise monomeric in the solid state.

Concluding Remarks

Findings presented here corroborate the proposal of a bimetallic mechanism (Scheme 1) with an observable intermediate, for dinitrogen cleavage by three-coordinate molybdenum(III) amide complexes. The purple, thermally-unstable intermediate (μ-N$_2$){Mo[N(R)Ar]$_3$}$_2$ was found to convert to the nitrido product, NMo[N(R)Ar]$_3$, according to a first-order kinetic profile over the temperature range interrogated (25−65 °C). Temperature-dependent kinetic isotope effect data obtained for breakup of the isotopomer (μ-^{15}N$_2$){Mo[N(R)Ar]$_3$}$_2$ are in line with rate-determining NN bond cleavage. A Raman spectroscopic investigation of (μ-N$_2$){Mo[N(R)Ar]$_3$}$_2$ and its ^{15}N$_2$ isotopomer suggests an NN bond order of ca. 2 for these complexes. EXAFS characterization of (μ-N$_2$){Mo[N(R)Ar]$_3$}$_2$ indicates a linear MoNNMo linkage in this μ-dinitrogen complex, an assignment corroborated by a temperature-dependent magnetic susceptibility study indicating a triplet ground state for (μ-N$_2$){Mo[N(*t*-Bu)Ph]$_3$}$_2$. EXAFS structural characterization data pertaining to Mo[N(R)Ar]$_3$ and NMo[N(R)Ar]$_3$ are in accord with single-crystal X-ray structural data for Mo[N(R)Ar]$_3$ and NMo[N(*t*-Bu)Ph]$_3$.

(50) Johnson, M. J. A.; Odom, A. L.; Cummins, C. C.; Manuscript in preparation.

(51) Johnson, A. R.; Wanandi, P. W.; Cummins, C. C.; Davis, W. M. *Organometallics* **1994**, *13*, 2907.

(52) Odom, A. L.; Cummins, C. C.; Protasiewicz, J. D. *J. Am. Chem. Soc.* **1995**, *117*, 6613.

(53) Odom, A. L.; Cummins, C. C. *Organometallics* **1996**, *15*, 898.

The potential utility of three-coordinate molybdenum(III) complexes as models for biological nitrogen fixation[54] stems from the ease with which they can be used to probe the molecular-level details of dinitrogen binding, reduction, and cleavage. Especially attractive is the fact that sterically and electronically tunable three-coordinate molybdenum(III) complexes are now available for study in the context of fully synthetic dinitrogen cleavage systems. Catalytic dinitrogen cleavage systems based on the chemistry described here are in the offing if suitable N-atom transfer chemistries can be developed to convert molybdenum(VI) nitrido complexes into molybdenum(III) species active for dinitrogen cleavage.[3]

Experimental Section

General Details. Unless stated otherwise, all operations were performed in a Vacuum Atmospheres drybox under an atmosphere of purified nitrogen, or using standard Schlenk techniques under an argon atmosphere. Anhydrous ether and toluene were purchased from Mallinckrodt; *n*-pentane and *n*-hexane were purchased from EM Science. Ether was distilled under a nitrogen atmosphere from purple sodium benzophenone ketyl. Aliphatic hydrocarbon solvents were distilled under a nitrogen atmosphere from very dark blue to purple sodium benzophenone ketyl solubilized with a small quantity of tetraglyme. Toluene was refluxed over molten sodium for at least 2 days, prior to its distillation under a nitrogen atmosphere. Distilled solvents were transferred under vacuum into Teflon-stopcocked glass vessels and stored, prior to use, in a Vacuum Atmospheres drybox. Benzene-d_6 was degassed and dried over blue sodium benzophenone ketyl and transferred under vacuum into a storage vessel. Chloroform-*d* and toluene-d_8 were degassed and dried over 4-Å sieves. Alumina and 4-Å sieves were activated *in vacuo* overnight at a temperature above 180 °C. Li[N(R)Ar](OEt$_2$),[22] HN(*t*-Bu)Ph,[55] *mer*-MoCl$_3$(THF)$_3$,[21] and mesityl azide[56] were prepared according to published procedures. Other chemicals were used as received. Infrared spectra were recorded on a Perkin-Elmer 1600 Series FTIR. UV−visible spectra were recorded on a Hewlett-Packard 8453 diode-array spectrophotometer. ^{1}H and ^{13}C NMR spectra were recorded on Varian XL-500, Varian XL-300, or Varian Unity-300 spectrometers. ^{1}H and ^{13}C chemical shifts are reported with reference to solvent resonances (residual C$_6$D$_5$*H* in C$_6$D$_6$, 7.15 ppm; *C*$_6$D$_6$, 128.0 ppm; C*H*Cl$_3$ in CDCl$_3$, 7.24 ppm; *C*DCl$_3$, 77.0 ppm) and were recorded at ca. 25 °C unless otherwise indicated. ^{2}H chemical shifts are reported with respect to external C$_6$D$_6$ (7.15 ppm). ^{15}N chemical shifts are reported with respect to external nitromethane at 380.2 ppm (relative to liquid NH$_3$ at 0 ppm). Solution magnetic susceptibilities were determined by ^{1}H NMR at 300 MHz using the method of Evans.[23] Routine coupling constants are not reported. Combustion analyses (C, H, and N) were performed by Oneida Research Services, Whitesboro, NY. Melting points were obtained in sealed glass capillaries and are uncorrected.

Synthesis of Mo[N(R)Ar]$_3$. In a typical preparation, *mer*-MoCl$_3$(THF)$_3$ (1.743 g, 4.164 mmol) and Li[N(R)Ar](OEt$_2$) (2.190 g, 8.315 mmol) were added to 70 mL of cold (−100 °C) ether, and the mixture was stirred for 2.5 h after being warmed to 28 °C. The precipitated LiCl and excess *mer*-MoCl$_3$(THF)$_3$ were removed by filtration. Analysis of the filtrate by ^{2}H NMR spectroscopy showed only one major product, with a relatively sharp ($\Delta\nu_{1/2}$ = 35 Hz) signal at 64.6 ppm corresponding to the ^{2}H-labeled *tert*-butyl groups in paramagnetic Mo[N(R)Ar]$_3$. The filtrate was concentrated and cooled to −35 °C under an argon atmosphere to produce orange-red, crystalline Mo[N(R)Ar]$_3$ (mp 126−128 °C, yield 1.247 g, 1.940 mmol, 70%). Mo[N(R)Ar]$_3$ is extremely oxygen- and moisture-sensitive, but decomposes <5% at 25 °C in an inert atmosphere over 24 h. ^{1}H NMR (C$_6$D$_6$): 64.0 (C(CD$_3$)$_2$C*H*$_3$), ca. 23 (br, ortho Ar*H*), −9.63 (ArC*H*$_3$), −51.67 ppm (br, para Ar*H*). Anal. Calcd for C$_{36}$H$_{36}$D$_{18}$MoN$_3$: C, 67.26; H, 8.47; N, 6.54. Found: C, 67.61; H, 8.38; N, 6.40.

SQUID Magnetic Measurements on Mo[N(R)Ar]$_3$. Measurements were made using a Quantum Design SQUID magnetometer. The magnetometer uses the MPMSR2 software (Magnetic Property Measurement System Revision 2). Data were recorded at a field strength of 5000 G. Gel caps (Gelatin Capsule No. 4 Clear) and straws were ordered from Quantum Design, Inc.

Samples of Mo[N(R)Ar]$_3$ for magnetic measurements were prepared in the drybox as described above. The solid compound was placed into a preweighed gel cap, and a preweighed plug of Parafilm was inserted above it, to keep it in place. The mass of the Mo[N(R)Ar]$_3$ sample was then ascertained by weighing the loaded gel cap. The loaded gel cap was mounted in a straw, and the straw was placed in an N$_2$-filled vessel for transport to the magnetometer. The straw was placed on the end of a rod for insertion into the magnetometer. The field and temperature were adjusted to 5000 G and 5 K, respectively. Once the temperature had equilibrated and the field was stable, the sample was centered. This was done by running a full-length DC scan, adjusting the position automatically, and then recentering using a DC centering scan. During the run, measurements were taken over the following temperature ranges with the indicated increments: 5−10 K (one data point every 1 K), 12−20 K (one data point every 2 K), 23−50 K (one data point every 3 K), 55−100 (one data point every 5 K), 110−200 K (one data point every 10 K), 220−300 K (one data point every 20 K). The run required approximately 5 h.

The data for Mo[N(R)Ar]$_3$ fit the Curie−Weiss law in the temperature range 5−300 K (R = 0.999 87). The calculated curve (Figure 1) is the best least-squares fit of the observed susceptibility data to the equation $\chi_M(\text{obs}) = ((\mu^2)/(7.997584(T - \theta))) - C$. The value of μ obtained in this manner was 3.82 μ_B, to be compared with the spin-only value for three unpaired electrons, 3.87 μ_B. In the least-squares fit, carried out using the General curve-fitting routine included with the program Kaleidagraph, both θ and C were treated as variable parameters. The obtained value of θ, the Weiss constant, was −2.8755 K. The value of the constant C, included to represent the sum of all temperature-independent contributions to the total observed susceptibility, including the diamagnetic correction and temperature-independent paramagnetism, was −0.000 632 06. The raw data plotted in Figure 1 are deposited in the supporting information.

X-ray Crystal Structure of Mo[N(R)Ar]$_3$. The crystal and structure refinement data in this section have been communicated in part[2] and are deposited here for completeness. An orange parallelepiped crystal of approximate dimensions 0.24 × 0.32 × 0.32 mm was obtained by cooling an ether solution to −35 °C. The crystal was coated with Paratone-N oil and mounted on a glass fiber in a stream of cold N$_2$. Data collection was carried out at −86 °C on an Enraf-Nonius CAD-4 diffractometer with graphite-monochromated Mo Kα radiation. A total of 9653 reflections were collected to a 2θ value of 44.9°, of which 9186 were unique (R_{int} = 0.051). The structure was solved by direct methods. Non-hydrogen atoms were refined anisotropically. The final cycle of full-matrix least-squares refinement was based on 5584 observed reflections ($I > 3.00\sigma(I)$) and 722 variable parameters and converged (largest parameter shift was 0.16 times its esd) with R = 0.066 and R_w = 0.065. A final difference Fourier map showed no chemically significant features. Crystal data are a = 13.736(4) Å, b = 15.948(4) Å, c = 16.187(7) Å, α = 88.93(2)°, β = 84.46(2)°, γ = 88.35(2)°, V = 3527(4) Å^3, space group $P\bar{1}$, Z = 4, molecular weight = 642.90 for C$_{36}$H$_{36}$D$_{18}$N$_3$Mo, and d(calcd) = 1.210 g/cm^3.

Kinetic Studies: Conversion of (μ-N$_2$){Mo[N(R)Ar]$_3$}$_2$ to 2 NMo[N(R)Ar]$_3$ and of (μ-^{15}N$_2$){Mo[N(R)Ar]$_3$}$_2$ to 2 ^{15}NMo[N(R)Ar]$_3$. Stock solutions of (μ-N$_2$){Mo[N(R)Ar]$_3$}$_2$ were prepared according to the following typical procedure. Toluene (5.0 g) was added to 251 mg of Mo[N(R)Ar]$_3$ (0.390 mmol), giving an approximately 0.4 M solution. The solution, in a 20-mL scintillation vial having a hole in its cap, was then stored in the glovebox refrigerator under ca. 1 atm of N$_2$ at −35 °C for ca. 10 days. During this time the reaction mixture

(54) (a) Kim, J.; Rees, D. C. *Biochemistry* **1994**, *33*, 389. (b) Kim, J.; Woo, D.; Rees, D. C. *Biochemistry* **1993**, *32*, 7104. (c) Rees, D. C.; Kim, J.; Georgiadis, M. M.; Komiya, H.; Chirino, A. J.; Wood, D.; Schlessman, J.; Chan, M. K.; Joshuator, L.; Santillan, G.; Chakrabarti, P.; Hsu, B. T. *ACS Symp. Ser.* **1993**, *535*, 170. (d) Chan, M. K.; Kim, J. S.; Rees, D. C. *Science* **1993**, *260*, 792. (e) Georgiadis, M. M.; Komiya, H.; Chakrabarti, P.; Woo, D.; Kornuc, J. J.; Rees, D. C. *Science* **1992**, *257*, 1653. (f) Kim, J. S.; Rees, D. C. *Science* **1992**, *257*, 1677. (g) Kim, J. S.; Rees, D. C. *Nature* **1992**, *360*, 553. (h) Howard, J. B.; Rees, D. C. *Adv. Protein Chem.* **1991**, *42*, 199. (i) Bolin, J. T.; Ronco, A. E.; Morgan, T. V.; Mortenson, L. E.; Xuing, N.-H. *Proc. Natl. Acad. U.S.A.* **1993**, *90*, 1078.

(55) Biehl, E. R.; Smith, S. M.; Reeves, P. C. *J. Org. Chem.* **1971**, *36*, 1841.

(56) Ugi, I.; Perlinger, H.; Behringer, L. *Chem. Ber.* **1958**, *91*, 2330.

acquired a rich purple color ($\lambda_{max} = 547$ nm). Stock solutions of (μ-$^{15}N_2$){Mo[N(R)Ar]$_3$}$_2$ were prepared according to the following typical procedure. A 0.1-L glass tube containing 1 atm of $^{15}N_2$ (98+% isotopic purity) at STP was purchased from Cambridge Isotopes Laboratory, and to the cylinder was attached, by glass-blowing techniques, an in-line Chemglass Teflon stopcock suitable for attachment to a vacuum or gas system via a hose. Into the small space (ca. 5 mL) between the breakseal and the Teflon stopcock was added a magnetic bar (to break the breakseal) and a solution of Mo[N(R)Ar]$_3$ (50 mg, 0.078 mmol) in toluene (1.0 g). The solution was then carefully degassed for ca. 30 s by exposure to dynamic vacuum. The stopcock was tightly closed to isolate the Mo[N(R)Ar]$_3$ solution in the evacuated space, and then the magnetic bar was addressed via an external magnet and manipulated to break the breakseal, admitting $^{15}N_2$ into the region containing the Mo[N(R)Ar]$_3$ solution. The whole assembly was then placed in the glovebox refrigerator at −35 °C. After a few minutes, and thereafter periodically, the stopcock was checked for a tight closure, as Teflon may shrink upon cooling. After at least 6 days the purple solution was removed from the vessel using a disposable 1-mL syringe fitted with a long steel needle. The stock solution was stored thereafter in a scintillation vial at −35 °C.

Aliquots from the stock solutions were diluted for kinetic measurements. Data collection began when the band at 547 nm had decayed to ca. 1.3 absorbance units. Data were collected on an Hewlett-Packard HP 8453 diode array spectrophotometer. The reaction temperature was controlled to within ±0.5 °C using an HP 89090A Peltier temperature control accessory. The decay of purple (μ-N_2){Mo[N(R)Ar]$_3$}$_2$ was monitored at $\lambda_{max} = 547$ nm. The amber product NMo[N(R)Ar]$_3$ does not absorb in this region. Samples were stirred at 250 rpm by an internal Teflon-coated magnetic stir bar and allowed to equilibrate at the desired temperature for 120 s prior to data acquisition. In a typical run, between 700 and 1000 data points were processed and used to determine rates. Between 25 and 65 °C, plots of $\ln(A-A_\infty)$ vs time were linear through at least 4 half-lives. Rate constants used as data points in the Eyring plot (Figure 11) were determined using the Kaleidagraph least-squares curve-fitting routine, using the equation $A = A_\infty + A_0[\exp(-kt)]$. From three to six runs were carried out at each temperature, and the reported rate constants are unweighted averages. The error associated with each rate constant was estimated from the reproducibility and is reported at the 95% confidence interval.[57] Raw rate data are deposited in the supporting information.

EXAFS Sample Preparation: (μ-N_2){Mo[N(R)Ar]$_3$}$_2$. A solution of Mo[N(R)Ar]$_3$ (1.16 g, 1.80 mmol) in 9.0 g of toluene was stored in a −35 °C glovebox refrigerator under ca. 1 atm of dinitrogen. After 6 days an aliquot of the deep purple solution was removed for ^{2}H NMR analysis, revealing a 1:3 ratio of the resonances at 64 and 14 ppm, which we assign respectively to Mo[N(R)Ar]$_3$ and (μ-N_2){Mo[N(R)Ar]$_3$}$_2$. The extent of conversion was probably greater than 75% based on Mo, in view of the fact that some purple solid, presumably (μ-N_2){Mo[N(R)Ar]$_3$}$_2$, was observed to have precipitated. Three rectangular EXAFS cells (Pyrex, 2 × 1 × 1 cm) were filled with the cold purple solution, degassed, and flame-sealed with a hand torch, the sample being kept covered with powdered dry ice throughout. **Mo[N(R)Ar]$_3$.** An EXAFS cell (Pyrex, 2 × 1 × 1 cm) was loaded with a solution of Mo[N(R)Ar]$_3$ (0.168 mmol, 108 mg) in ca. 2 mL of toluene, degassed, and flame-sealed with a hand torch, the sample being kept covered with powdered dry ice throughout. **NMo[N(R)Ar]$_3$.** An EXAFS cell (Pyrex, 2 × 1 × 1 cm) was loaded with a solution of NMo[N(R)Ar]$_3$ (0.152 mmol, 100 mg) in ca. 2 mL of toluene, degassed, and flame-sealed with a hand torch, the sample being kept covered with powdered dry ice throughout. The samples were shipped, on dry ice, from MIT to Stanford's SLAC via Federal Express.

EXAFS Data Collection. X-ray absorption spectroscopy measurements were carried out at the Stanford Synchrotron Radiation Laboratory with the SPEAR storage ring containing 55−90 mA at 3.0 GeV. Molybdenum K-edge X-ray absorption spectra were collected on beamline 7-3 using a Si(220) double crystal monochromator with an upstream vertical aperture of 1 mm and a wiggler field of 1.8 T. Harmonic rejection was accomplished by detuning one monochromator crystal to approximately 50% off-peak, and no specular optics were present in the beamline. X-ray absorption was measured in transmittance using argon-filled ionization chambers. A spectrum of molybdenum foil was collected simultaneously with that of the sample, and spectra were calibrated with reference to the lowest energy inflection point of the foil, assumed to be 20 003.9 eV.

During data collection, the samples of (μ-N_2){Mo[N(R)Ar]$_3$}$_2$ and NMo[N(R)Ar]$_3$ were maintained at a temperature of approximately 10 K, using an Oxford Instruments liquid helium flow cryostat. The sample Mo[N(R)Ar]$_3$ was discovered to reversibly crystallize from solution at low temperatures and therefore was maintained at the higher temperature of 200 K in order to maintain a solution.

EXAFS Data Analysis. The data were analyzed using the EXAFSPAK suite of computer programs[58] running on Digital Equipment Corp. VAXstation 4000 and AXP graphics workstations. The EXAFS oscillations $\chi(k)$ were quantitatively analyzed by curve-fitting.[59] The EXAFS total amplitude and phase-shift functions were calculated using the program *feff* (version 6.01) of Rehr and co-workers.[29] **Mo[N(R)Ar]$_3$.** The EXAFS spectrum of Mo[N(R)Ar]$_3$ was fitted with reference to the known crystal structure. Coordinates from the −86 °C crystal structure (see above) were used in *feff* to calculate accurate phase, amplitude, and mean free path functions. These functions were then used to refine interatomic distances in the 200 K solution form of Mo[N(R)Ar]$_3$. Of the many scattering paths generated by *feff*, only five were found to contribute sufficient intensity to merit inclusion in the refinement, specifically the single-scattering contributions from the central carbon of the R group and from three carbons of the Ar group, in addition to the coordinating nitrogen. **NMo[N(R)Ar]$_3$.** The spectrum of NMo[N(R)Ar]$_3$ was fitted assuming a very similar ligand structure to that of Mo[N(R)Ar]$_3$. The phase, amplitude, and mean free path functions calculated for the ligand interactions of Mo[N(R)Ar]$_3$ were also used for NMo[N(R)Ar]$_3$, and the same numbers of shells were included. The first shell Mo−N and Mo≡N distances were iteratively refined and new functions calculated until no further change was observed. **(μ-N_2){Mo[N(R)Ar]$_3$}$_2$.** The spectrum of (μ-N_2){Mo[N(R)Ar]$_3$}$_2$ was also fitted in part using the calculated phase, amplitude, and mean free path functions calculated for Mo[N(R)Ar]$_3$. In this case, some of the parameters were fixed at the mean of values derived from Mo[N(R)Ar]$_3$ and NMo[N(R)Ar]$_3$. These were the offset to $k = 0$, E_0, and the distances to three of the outer carbons (which contribute only subtly to the total EXAFS); this was done in order to eliminate correlations in the minimization, and fits in which these variables were floated independently yielded values which differed only slightly from the mean values used. In addition, the highly correlated Debye−Waller factors for the two Mo−N shells were refined as a single parameter with values proportional to their distances [justification for this approximation is found in the values of the independently-refined Debye−Waller factors for the Mo−N interactions of NMo[N(R)Ar]$_3$]. Phase, amplitude, and mean free path functions for the MoNNMo molecular unit were calculated using *feff* by postulating a starting (linear) coordinate model, then iteratively refining the distances, deriving new coordinates, and recalculating functions until no further difference was found. In this case, substantial multiple-scattering contributions to the outer shells of the linear molecule were predicted and were included in the fit. In the final analysis, all three interatomic distances Mo−N, Mo···N, and Mo···Mo were floated and excellent agreement between them, assuming a linear model, was found. Deuterium NMR of the (μ-N_2){Mo[N(R)Ar]$_3$}$_2$ sample showed a purity of 75% (based on Mo, see above), the remainder being the starting material Mo[N(R)Ar]$_3$, and therefore appropriate coordination numbers for the MoNNMo

(57) Wilson, E. B., Jr. *An Introduction to Scientific Research*; Dover: New York, 1990. See especially pages 239−242 where a description of Student's *t* distribution can be found.

(58) The EXAFSPAK program suite was developed by one of the authors (G.N.G.) and is available from him by application in writing.

(59) The EXAFS oscillations $\chi(k)$ are given by the approximate equation:

$$\sum_{i=1}^{n} \frac{N_i A_i(k,R_i)}{kR_i^2} e^{-2R_i/\lambda_i(k,R_i)} e^{-2\sigma_i^2 k_i^2} \sin[2kR_i + \alpha_i(k,R_i)]$$

where k is the photoelectron wave number and $A_i(k,R_i)$ and $\alpha_i(k,R_i)$ are the EXAFS total amplitude and total phase-shift functions, respectively, for scattering path i. N_i is the degeneracy of scattering path i with a total path length R_i. $\lambda_i(k,R_i)$ is the photoelectron mean free path function, and σ_i^2 is the Debye−Waller factor (the mean square deviation of R_i). The summation is over all sets of nondegenerate scattering paths.

were reduced accordingly (the assumption, borne out by the final fit results, being that the ligand contribution is very little changed between $Mo[N(R)Ar]_3$ and $(\mu\text{-}N_2)\{Mo[N(R)Ar]_3\}_2$).

Raman Spectra of $(\mu\text{-}N_2)\{Mo[N(R)Ar]_3\}_2$ and $(\mu\text{-}^{15}N_2)\{Mo[N(R)Ar]_3\}_2$. Samples of the two species were generated as described above for the kinetic measurements. Spectra were obtained at room temperature, as liquid samples at approximately the concentration of the toluene stock solutions, and were taken quickly in order to minimize decomposition to the corresponding terminal nitrido species. The solution Raman spectra were recorded on a Spex 1677 (0.6 mm) monochromator equipped with a Princeton Instruments, back thinned 512 × 512 liquid nitrogen cooled CCD detector. Excitation was with a Coherent I-90-K krypton ion laser (647 nm) operating at a power of 20 mW. The plasma lines were cut off with an Applied Photophysics laser filter monochromator. Laser radiation from the scattered light was removed with a Kaiser Optical Systems holographic notch filter. Optimal Raman spectra were obtained with 100-μm slits. Calibration was obtained with the 1662- and 1404-cm^{-1} bands of DMF (dimethylformamide). The data for the two samples and for the toluene background were imported into the program Kaleidagraph. The toluene spectrum was subtracted using an appropriate scaling factor; no other manipulations were applied to the data.

Synthesis of $NMo[N(R)Ar]_3$ from $Mo[N(R)Ar]_3$ and Dinitrogen. A preparative-scale reaction between $Mo[N(R)Ar]_3$ and dinitrogen (ca. 1 atm in a glovebox) was conducted by storing a solution of $Mo[N(R)Ar]_3$ (300 mg, 0.467 mmol) in toluene (6 mL) at −35 °C for ca. 76 h. The reaction's progress was monitored occasionally by ^2H NMR. Aliquots used for monitoring progress were returned to the reaction mixture so as not to diminish the yield. When conversion of $Mo[N(R)Ar]_3$ (signal at 64 ppm) to $(\mu\text{-}N_2)\{Mo[N(R)Ar]_3\}_2$ (signal at 14 ppm) was judged complete, the reaction mixture was allowed to warm to room temperature (ca. 28 °C) for 5 h, during which time the purple color dissipated and the mixture turned amber. ^1H NMR analysis of the crude material obtained upon removing volatile matter revealed that $NMo[N(R)Ar]_3$ had formed cleanly. The nitrido complex $NMo[N(R)Ar]_3$ was isolated in 76% yield (0.233 g, 0.355 mmol) upon recrystallization (Et_2O, −35 °C). The sample of $NMo[N(R)Ar]_3$ so prepared was identical in its spectroscopic and physical properties to samples of $NMo[N(R)Ar]_3$ prepared by other means (see following paragraph). IR and ^{15}N NMR data for samples of $^{15}NMo[N(R)Ar]_3$ prepared from $Mo[N(R)Ar]_3$ and 1 atm of 99% $^{15}N_2$ (see procedure above for generation of $(\mu\text{-}^{15}N_2)\{Mo[N(R)Ar]_3\}_2$) were identical to those reported below for $^{15}NMo[N(R)Ar]_3$ prepared from $Mo[N(R)Ar]_3$ and $^{15}NNN(p\text{-}C_6H_4Me)$.

Synthesis of $NMo[N(R)Ar]_3$ from $Mo[N(R)Ar]_3$ and Mesityl Azide. A solution of $Mo[N(R)Ar]_3$ (0.686 mmol, 441 mg) in 7 mL of Et_2O at 25 °C was added to a stirred solution of mesityl azide (161 mg, 0.997 mmol) in 3 mL of Et_2O. Volatile material was removed *in vacuo* after 30 min at 30 °C. Pure amber $NMo[N(R)Ar]_3$ was obtained in 73% yield (0.501 mmol, 329 mg) after one recrystallization (Et_2O, −35 °C). ^1H NMR (C_6D_6): 6.61 (s, 3H, para Ar*H*), 5.94 (s, 6H, ortho Ar*H*), 2.03 (s, 18H, ArCH_3), 1.62 (s, 9H, C$(CD_3)_2CH_3$). ^{13}C NMR (C_6D_6): 150.69 (s, aryl *ipso*), 137.10 (q, aryl meta), 128.84 (d, aryl ortho or para), 61.04 (s, *C*$(CD_3)_2CH_3$), 33.06 (q, C$(CD_3)_2$*C*H_3), 32.55 (m, C(*C*$D_3)_2CH_3$), 21.34 (q, aryl meta *C*H_3); one missing peak (d, aryl ortho or para) was not located and is presumed to have been obscured by the C_6D_6 signal. IR (KBr windows, pentane solution): 1042 cm^{-1} ν(MoN). Anal. Calcd for $C_{36}H_{36}D_{18}MoN_4$: C, 65.82; H, 8.29; N, 8.53. Found: C, 66.14; H, 7.90; N, 8.45. HRMS (M^+): calcd 658.45140, obsd 658.44713.

Synthesis of $^{15}NMo[N(R)Ar]_3$ from $Mo[N(R)Ar]_3$ and $^{15}NNN(p\text{-}C_6H_4Me)$. Terminally-$^{15}N$-labeled *p*-tolyl azide was prepared by the (slightly modified) method[60] of Hillhouse, Goeden, and Haymore: to a 50-mL Erlenmeyer flask containing a magnetic stir bar was added 1.2127 g of *p*-tolylhydrazine hydrochloride (7.645 mmol), 7 mL of distilled water, 2 mL of concentrated HCl, and ca. 5 mL of ether. The mixture was chilled to 0 °C, and $Na^{15}NO_2$ (0.5457 g, 7.796 mmol), as a solution in ca. 4 mL of chilled distilled water, was added over ca. 0.5 h dropwise via pipet. After all the $Na^{15}NO_2$ solution had been added, additional ether was added (ca. 5 mL), and the mixture was stirred and allowed to warm to ca. 10 °C. The aqueous layer was removed via pipet, and then the yellow solution containing $^{15}NNN(p\text{-}C_6H_4Me)$ was filtered through a plug of anhydrous sodium sulfate, in a pipet, into a flask for evaporation of volatile material. The solution was kept chilled (ice water bath) while volatile matter was removed *in vacuo*. The crude $^{15}NNN(p\text{-}C_6H_4Me)$ was brought directly into the glovebox, where it was weighed (550 mg, 4.13 mmol, 54%). A stock solution of 550 mg of $^{15}NNN(p\text{-}C_6H_4Me)$ in 9.2 g of cold ether was prepared, and stored at −35 °C. The ^1H NMR spectrum (C_6D_6) of the crude $^{15}NNN(p\text{-}C_6H_4Me)$ was recorded: δ = 6.685 (d, Ar*H*), 6.753 (d, Ar*H*), 1.964 (s, ArCH_3); this showed the crude material to be ca. 90% pure. GCMS analysis was also consistent with assignment of the major component of the crude product as $^{15}NNN(p\text{-}C_6H_4Me)$. A solution of $Mo[N(R)Ar]_3$ (480 mg, 0.75 mmol) in ca. 7 mL of Et_2O was added dropwise, via pipet, to a stirred orange solution of $^{15}NNN(p\text{-}C_6H_4Me)$ (ca. 210 mg, 1.57 mmol, from a stock solution prepared as described above). During the addition, the color of the reaction mixture was purple. After ca. 5 more min, the color of the reaction mixture was brown. After the volume of the reaction mixure was reduced to ca. 4 mL, it was stored at −35 °C, leading to the formation of dark crystalline solid (160 mg isolated, 0.243 mmol, 32%). HRMS (M^+): calcd 659.44843, obsd 659.44595. ^{15}N NMR (50.659 MHz): 840 ppm (s). ^1H NMR: as reported above for $NMo[N(R)Ar]_3$. IR (KBr solution cells, pentane): $\nu(Mo^{15}N)$ = 1014 cm^{-1} (calcd 1011 cm^{-1}); the 1042 cm^{-1} band attributed to ν(MoN) for the unlabeled derivative was absent from this spectrum.

Preparation of Li[N(*t*-Bu)Ph](OEt$_2$). A solution of HN(*t*-Bu)Ph, 20.0 g (0.134 mol), in a mixture of ether (40 mL) and pentane (95 mL) in a 500-mL Erlenmeyer flask was frozen solid in the glovebox cold well. The vessel was removed from the well, and upon partial thawing, a hexanes solution of *n*-butyllithium (92 mL, 1.6 M, 0.15 mol, 1.1 equiv) was added via pipet. The reaction mixture was stirred for 4 h, with warming to ca. 28 °C. The mixture acquired a pale orange color. The resulting solution was concentrated to ca. 50 mL under vacuum, eliciting precipitation of the product as a white powder. The powder was collected on a sintered glass frit, washed with pentane, and dried under vacuum (21.0 g, 0.0916 mol, 68.3%). The material thus obtained was >95% pure according to ^1H NMR spectroscopy. ^1H NMR (300 MHz, C_6D_6, 20.8 °C): δ = 7.198 ("t" [dd], 2H, Ph meta), 6.879 (d, 2H, Ph ortho), 6.474 (t, 1H, Ph para), 3.092 (q, 4H, O(CH_2-$CH_3)_2$), 1.552 (s, 9H, C(C$H_3)_3$), 0.865 (t, 6H, O(CH_2C$H_3)_2$). $^{13}C\{^1H\}$ NMR (75 MHz, C_6D_6, 20.8 °C): δ = 159.24 (Ph *ipso*), 129.92 (Ph ortho), 118.03 (Ph meta), 110.83 (Ph para), 65.124 (O(*C*$H_2CH_3)_2$), 52.452 (*C*$(CH_3)_3$), 31.528 (C(*C*$H_3)_3$), 14.651 (O(CH_2*C*$H_3)_2$).

Synthesis of Mo[N(*t*-Bu)Ph]$_3$. To argon-sparged ether (100 mL) were added sequentially Li[N(*t*-Bu)Ph](OEt$_2$) (6.00 g, 26.2 mmol, 3.00 equiv) and $MoCl_3(THF)_3$ (3.65 g, 8.72 mmol) as white and orange powders, respectively. The stirred reaction mixture was sparged with Ar for ca. 1 min, following which the reaction vessel was fitted with a rubber septum. The reaction mixture remained orange for ca. 5 min, presumably due to unreacted $MoCl_3(THF)_3$, before it suddenly adopted a dark mud-brown color. The mixture was stirred under an Ar atmosphere for 90 min, at which point a ^1H NMR spectrum of an aliquot indicated that the major constituent species was the desired Mo[N(*t*-Bu)Ph]$_3$ (see below for spectral data). After being stirred for a total of 2 h, the reaction mixture was vacuum filtered through a bed of Celite on a sintered glass frit. Volatile material was removed from the filtrate *in vacuo*, providing a dark brown solid. The solid was dissolved in ether (ca. 15 mL), and the resulting solution was sparged with argon for several minutes. The container was tightly sealed and stored at −35 °C overnight, giving a crop of translucent burgundy crystals (1.54 g, 32.7%). The mother liquor was concentrated *in vacuo* and stored again at −35 °C to provide a second crop of burgundy crystals. Yield of spectroscopically pure Mo[N(*t*-Bu)Ph]$_3$: 2.61 g (55.4%). ^1H NMR (300 MHz, C_6D_6, 22 °C): δ = 66.5 (br, 27H, *t*-Bu), 22.4 (br, 6H, Ph meta or ortho), −23.0 (br, 6H, Ph meta or ortho), −49.8 (br, 3H, Ph para). μ_{eff} (300 MHz, C_7D_8, 23 °C): 3.41 μ_B. We have not obtained a satisfactory combustion analysis for this thermally-sensitive compound; the following are typical results. Anal. Calcd for $C_{30}H_{42}MoN_3$: C, 66.65; H, 7.83; N, 7.77. Found: C, 67.80; H, 8.63; N, 7.55.

(60) Hillhouse, G. L.; Goeden, G. V.; Haymore, B. L. *Inorg. Chem.* **1982**, *21*, 2064.

SQUID Measurements on (μ-N_2){Mo[N(*t*-Bu)Ph]$_3$}$_2$. The sample was obtained in the following way. A saturated solution of Mo[N(*t*-Bu)Ph]$_3$ in pentane at −35 °C was stored in a vial capped by a septum pierced by a needle to permit dinitrogen influx. Over the course of 2 days, the solution acquired a dark purple color, and a fine, intensely purple-black microcrystalline solid presumed to be (μ-N_2){Mo[N(*t*-Bu)Ph]$_3$}$_2$ began to precipitate. The supernatant was transferred to another vial and treated similarly to obtain further crops. The solid was washed with cold (−35 °C) ether and pumped to dryness before being stored at −35 °C. Purity was assayed via integration on the ^{1}H NMR spectrum of a sample dissolved in C_6D_6. Only (μ-N_2){Mo[N(*t*-Bu)Ph]$_3$}$_2$ and NMo[N(*t*-Bu)Ph]$_3$ were observed; no Mo[N(*t*-Bu)Ph]$_3$ was present. ^{1}H NMR (300 MHz, C_6D_6, 20 °C): δ = 12.62 (br s [$\Delta\nu_{1/2}$ = 33 Hz], 9H, C(C*H*$_3$)$_3$), ca. 9.8 (br s [$\Delta\nu_{1/2}$ = 316 Hz], 2H, phenyl ortho or meta), ca. 3.8 (br s [$\Delta\nu_{1/2}$ = 175 Hz], 2H, phenyl ortho or meta), 2.36 (br s [$\Delta\nu_{1/2}$ = 22 Hz], 1H, phenyl para). ^{13}C{^{1}H} and ^{13}C NMR (75.4 MHz, $CDCl_3$, 22 °C): no peaks observed.

Squid magnetic measurements on samples of (μ-N_2){Mo[N(*t*-Bu)Ph]$_3$}$_2$ were made as described for Mo[N(R)Ar]$_3$ (*vide supra*).

The data for (μ-N_2){Mo[N(*t*-Bu)Ph]$_3$}$_2$ fit the Curie−Weiss law in the temperature range 29−300 K (R = 0.999 82). The calculated curve (Figure 8) is the best least-squares fit of the observed susceptibility data to the equation $\chi_M(\text{obs}) = ((\mu^2)/(7.997584(T - \theta))) - C$. The value of μ obtained in this manner was 2.85 μ_B, to be compared with the spin-only value for two unpaired electrons, 2.83 μ_B. In the least-squares fit, carried out using the General curve-fitting routine included with the program Kaleidagraph, both θ and C were treated as variable parameters. The obtained value of θ, the Weiss constant, was −14.626 K. The value of the constant C, included to represent the sum of all temperature-independent contributions to the total observed susceptibility, including the diamagnetic correction and temperature-independent paramagnetism, was −0.000 395 03. The raw data plotted in Figure 8 are deposited in the supporting information.

Synthesis of NMo[N(*t*-Bu)Ph]$_3$ from Mo[N(*t*-Bu)Ph]$_3$ and Mesityl Azide. Neat mesityl azide (199.3 mg, 1.236 mmol, 1.33 equiv) was added to a stirred orange-brown solution of Mo[N(*t*-Bu)Ph]$_3$ (501.3 mg, 0.9273 mmol) in ether (10 mL) at −35 °C. The reaction mixture acquired a dark purple color very rapidly; this color faded substantially but did not entirely disappear as the mixture was stirred at 29 °C for 3 h. Ether was then removed *in vacuo*, and the resulting dark solid crystallized from ether at −35 °C. Recrystallization from ether delivered pure NMo[N(*t*-Bu)Ph]$_3$ as transparent yellow-orange crystals (374.6 mg [two crops], 0.6754 mmol, 72.83%) suitable for an X-ray diffraction study. ^{1}H NMR (300 MHz, $CDCl_3$, 22 °C): δ = 7.031 (tt, 1H, para), 6.931 ("t" [dd], 2H, meta), 5.933 (d, 2H, ortho), 1.397 (s, 9H, C(C*H*$_3$)$_3$). ^{13}C{^{1}H} NMR (75.4 MHz, $CDCl_3$, 22 °C): δ = 150.44 (phenyl *ipso*), 130.42 (phenyl meta), 128.04 (phenyl ortho), 125.02 (phenyl para), 61.43 (*C*(CH$_3$)$_3$), 32.98 (C(*C*H$_3$)$_3$). ^{13}C NMR (75.4 MHz, $CDCl_3$, 22 °C): δ = 150.40 (s, phenyl *ipso*), 130.40 ("dt" [ddd], phenyl meta), 128.04 (dd, phenyl ortho), 125.02 (dt, phenyl para), 61.46 (s, *C*(CH$_3$)$_3$), 32.98 (q, C(*C*H$_3$)$_3$). Anal. Calcd for $C_{30}H_{42}MoN_4$: C, 64.97; H, 7.63; N, 10.10. Found: C, 64.79; H, 7.86; N, 10.18.

X-ray Crystal Structure of NMo[N(*t*-Bu)Ph]$_3$. Data were collected using a crystal of NMo[N(*t*-Bu)Ph]$_3$ having dimensions 0.5 × 0.4 × 0.4 mm. The crystal system was cubic, $a = b = c$ = 22.783(2) Å, and $\alpha = \beta = \gamma = 90°$, leading to a unit cell volume V = 11826(2) Å^3 with Z = 16. The space group was found to be I$\bar{4}$3d. The absorption coefficient was 0.467 mm^{-1}, the calculated density ρ = 1.246 g/cm^3, and $F(000)$ = 4672. Data were collected using a Siemens platform goniometer with a CCD detector at 208(2) K using molybdenum Kα radiation [λ = 0.710 73 Å] in the θ range 21.9−23.24° with limiting indices $-13 \le h \le 25$, $-18 \le k \le 25$, $-24 \le l \le 17$. Of the 12 790 reflections collected, 1415 were independent (R_{int} = 0.0372). A semiempirical absorption correction, from ψ scans, was applied. The structure was solved by direct methods (SHELXTL V5.0, Sheldrick, G. M., and Siemens Industrial Automation, Inc., 1995) in conjunction with standard difference Fourier techniques. Least-squares refinement based upon F^2 with 1413 data, zero restraints, and 107 parameters converged with final residuals: R_1 = 0.0247, wR_2 = 0.0491, and GOF = 1.265 based upon $I > 2\sigma(I)$. The largest peak and hole in the final difference Fourier map were respectively +0.149 and −0.191 e Å^{-3}.

Acknowledgment. This work made use of MRSEC Shared Facilities supported by the National Science Foundation under Award No. DMR-9400334. The Stanford Synchrotron Radiation Laboratory is funded by the Department of Energy, Office of Basic Energy Sciences. The Biotechnology Program is supported by the National Institutes of Health, Biomedical Research Technology Program, Division of Research Resources. Further support is provided by the Department of Energy, Office of Health and Environmental Research. We are indebted to Roger C. Prince of Exxon Research and Engineering Company for his assistance in data collection and Martin J. George of SSRL for use of his data collection software. We are also grateful to John Rehr of the University of Washington for providing us with a special extended *k*-range version of his program *feff*. Raman spectra were collected in the Harrison Spectroscopy Laboratory at MIT, supported in part by the National Institutes of Health. C.C.C. thanks Professors Richard R. Schrock and Barry K. Carpenter for helpful discussions. For funding, C.C.C. thanks the National Science Foundation (CAREER Award CHE-9501992), DuPont (Young Professor Award), the Packard Foundation (Packard Foundation Fellowship), Union Carbide (Innovation Recognition Award), and 3M (Innovation Fund Award). C.E.L. thanks MIT's UROP (Undergraduate Research Opportunities Program) for funding. M.J.A.J. is grateful for an NSERC graduate research fellowship.

Supporting Information Available: SQUID magnetic data for Mo[N(R)Ar]$_3$ and (μ-N_2){Mo[N(*t*-Bu)Ph]$_3$}$_2$, kinetic data for conversion of (μ-N_2){Mo[N(R)Ar]$_3$}$_2$ to 2 equiv of NMo[N(R)Ar]$_3$, kinetic data for the fragmentation of (μ-$^{15}N_2$){Mo[N(R)Ar]$_3$}$_2$ to 2 equiv of ^{15}NMo[N(R)Ar]$_3$, and tables of atom coordinates, anisotropic thermal parameters, and bond distances and angles for the X-ray structures of Mo[N(R)Ar]$_3$ and NMo[N(*t*-Bu)Ph]$_3$ (21 pages). See any current masthead page for ordering and Internet access instructions.

JA960574X